5-2019

IL-6/JAK1 DRIVES PD-L1 PHOSPHORYLATION AND GLYCOSYLATION TO PROMOTE CANCER IMMUNE EVASION

Li-Chuan Chan

IL-6/JAK1 DRIVES PD-L1 PHOSPHORYLATION AND GLYCOSYLATION TO PROMOTE CANCER IMMUNE EVASION

by

Li-Chuan Chan, B.V.M., M.S.

APPROVED:

_____
Mien-Chie Hung, Ph.D. Advisory Professor

_____
Paul J. Chiao, Ph.D.

_____
Ahmed Kaseb, M.D.

_____
Chunru Lin, Ph.D.

_____
Jeffrey T. Chang, Ph.D.

APPROVED:

_____

Dean, The University of Texas

MD Anderson Cancer Center UTHealth Graduate School of Biomedical Sciences

IL-6/JAK1 DRIVES PD-L1 PHOSPHORYLATION AND GLYCOSYLATION TO PROMOTE CANCER IMMUNE EVASION

A

DISSERTATION

Presented to the Faculty of

The University of Texas

MD Anderson Cancer Center UTHealth

Graduate School of Biomedical Sciences

in Partial Fulfillment

of the Requirements

for the Degree of

DOCTOR OF PHILOSOPHY

By

Li-Chuan Chan, B.V.M., M.S.

Houston, Texas

May, 2019

Dedication

This dissertation is dedicated to my mother and all of my family, and friends

who provided me their unconditional support and love in my life

Acknowledgments

I would like to express my deepest appreciation to all those who have encouraged and supported me during my Ph.D training. First, I would like to express my greatest gratitude to my advisor, Dr. Mien-Chie Hung, for being my role model of a scholar and a mentor. With his fully support and guidance, I learned how to think as a scientist and address important biomedical problems. In addition, he also teaches me how to be a modest person and face challenges optimistically, which will certainly benefit my future career and life. Second, I would like to thank all of my advisory committee members, Dr. Paul J. Chiao, Dr. Ahmed Kaseb, Dr. Chunru Lin, and Dr. Jeffrey T. Chang. They spend tremendous amount of time to provide me their experiences and valuable advices for improving my research skills. Third, I would like to express my sincere appreciation to my friends and colleagues who have helped me when I am pursuing Ph.D degree, especially to Dr. Chia-Wei Li, Dr. Jun-Mao Hsu, Dr. Heng-Huan Lee, Dr. Jong-Ho Cha, Dr. Wen-Hao Yang, Dr. Chao-Kai Chou, Dr. Yongkun Wei, Dr. Lei Nie, Dr. Weiya Xia and Dr. Jennifer L. Hsu. I also thank Su Zhang, Zhenbo Han, Jian Guan Shi, and Jin-Fong Lee for their daily assistance. Finally, I would like to give my sincere thanks to my mother and all of my family for supporting me with their love and care. They have always supported my career choices and encouraged me to overcome difficult moments.

IL-6/JAK1 DRIVES PD-L1 PHOSPHORYLATION AND GLYCOSYLATION TO PROMOTE CANCER IMMUNE EVASION

Li-Chuan Chan, B.V.M., M.S.

Advisory Professor: Mien-Chie Hung, Ph.D.

Glycosylation of immune receptors and ligands, such as T-cell receptor (TCR), major histocompatibility complex (MHC), and co-inhibitory molecules, regulates immune signaling activation, antigen presentation, and immune surveillance. Recent studies revealed that the glycan structures of co-inhibitory molecules are required for receptor-ligand interaction, a critical feature for activating cancer immune evasion. However, it is unclear how oncogenic signaling initiates glycosylation of co-inhibitory molecules to induce immunosuppression. Here we show interleukin (IL)-6-activated Janus kinase 1 (JAK1) phosphorylates programmed death-ligand 1 (PD-L1)-Tyr112, leading to the recruitment of endoplasmic reticulum (ER)-associated N-glycosyltransferase, STT3A, which catalyzes the glycosylation of PD-L1, contributing to its stability. A positive correlation between IL-6 and PD-L1 expression levels was observed in tumor samples from patients with hepatocellular carcinoma (HCC). Furthermore, IL-6 blockade led to downregulation of PD-L1 and increased sensitivity to anti-T-cell immunoglobulin mucin-3 (Tim-3) immune checkpoint therapies in animal models. These results identify a mechanism regulating initiation of PD-L1 glycosylation and suggest that the combination of anti-IL-6 and anti-Tim-3 is an effective, biomarker-driven, therapeutic strategy in HCC.

Table of Contents

List of Figures

List of Tables

CHAPTER 1. INTRODUCTION

1.1 Epidemiology and current therapeutic landscape of Hepatocellular carcinoma (HCC)

Liver cancer is the second most common cause of cancer death worldwide, and mortality rates due to liver cancer are steadily increasing. Hepatocellular carcinoma (HCC) and cholangiocarcinoma (CCA) are the two most frequent types of liver cancer, with more than 1 million newly diagnosed cases per year (1). HCC makes up approximately 90% of all primary liver cancers and usually develops in the context of chronic liver inflammation due to a variety of causes such as viral infections, heavy alcohol consumption, obesity, or nonalcoholic fatty liver disease (NAFLD) (2-9). The risk factors for HCC are well defined with 45% of diagnosed cases in US attributed to chronic hepatitis B and hepatitis C (HBV and HCV) infection. Among cases diagnosed in patients without evidence of chronic HBV or HCV infection, majority (55%) are due to excessive alcohol consumption, non-alcoholic steatohepatitis (NASH) and obesity (9, 10). The majority of patients with HCC cases are diagnosed at an advanced stage, where curative surgical treatment (resection or liver transplantation) is not possible and their only therapeutic option is palliative systemic therapy. The multi-kinase inhibitors sorafenib (front-line) and regorafenib (second-line) are targeted therapies approved by the U.S. Food and Drug Administration (FDA) for advanced HCC. However, overall response rates are low (2% and 10%, respectively) and, compared to placebo, the improvement in media overall survival was modest (~3 months) (9, 11). Therefore, there is an urgent and unmet need to develop; 1) novel therapeutic approaches that will improve overall survival for patients with HCC. 2) Decreasing rates of systemic and local recurrence by enhancing the effectiveness of immune surveillance in patients with HCC patients, and 3) suitable biomarkers for early detection through an in

depth analysis of molecular features and oncogenic pathways contributing totumorigenesis in HCC.(12).

Immunotherapeutic approaches inhibiting co-inhibitory ligand/receptor interaction and blocking immunosuppressive signaling in immune cells have resulted in significant survival benefit in patients across multiple tumor types (13). Multiple co-inhibitory receptors and ligands have been determined to contribute to the maintenance of immune evasion and immune dysfunction in HCC, including cytotoxic T-lymphocyte-associated protein 4 (CTLA-4)(14), programmed cell death protein-1 (PD-1) and its ligand (PD-L1), lymphocyte-activation gene 3 (LAG-3) and its ligand (MHC-II and fibrinogen-like protein 1)(15, 16), Tim-3 and its ligand (galectin-9)(17), and adenosine A2a receptor (A2aR) (18). The tumor microenvironment is the primary location that immune cells interact with and eliminate cancer cells (19) and blocking the interaction between PD-1 and PD-L1 on immune cells and cancer cells, respectively, is one of the major strategies for immune normalization in the tumor microenvironment (20). Notably, tumor cells expressing high levels of PD-L1 and exhausted infiltrating CD8(+) T cells were both enriched in tumor region of HCC patient samples (21). In addition, PD-L1 overexpression in the tumor microenvironment has been associated with tumor aggressiveness, poorer clinical outcome and postoperative recurrence in HCC (22). More recently, the PD-1 antibody nivolumab, was approved in the second line setting for the treatment of advanced HCC refractory to sorafenib on the basis of a 20% objective response rate in advanced HCC (23). While the approval of nivolumab represents an encouraging step forward in the treatment of HCC, more needs to be done to improve its efficacy in this setting. Because mechanism-driven, biomarker-guided combinatorial treatment strategies are generally considered to be an effective strategy to improve existing treatment paradigms (24, 25), uncovering the

mechanisms underlying the biosynthesis of PD-L1 and PD-1 may lead to the development of mechanism-driven immunotherapies that improve response rates and survival in patients with HCC.

Inflammation is a key component of the innate immune response and plays critical roles at different stages of tumorigenesis, including initiation, proliferation, angiogenesis, epithelial-mesenchymal transition, invasion, and metastasis. Furthermore, inflammation also affects cancer immune evasion and response to treatment (26-28). Multiple molecular pathways linked between cancer-associated inflammatory response and HCC have also be identified and these mechanisms have been proposed as therapeutic targets (26, 29, 30). Of note, high levels of inflammatory cytokine, IL-6, within the tumor or plasma has been correlated with poor prognosis in advanced HCC (31, 32). Mechanistically, IL-6 has been shown to promote cell proliferation, enhance tumor metastasis, and is required for tumor-initiating cell maintenance via the autocrine IL-6/LIN28 pathway (3, 4, 31, 33). Although it also has been reported that IL-6 signaling suppresses the antitumor immune response in tumor microenvironment, the underlying mechanism is not fully understood (7). Therefore, elucidating the role that IL-6 plays in regulating PD-L1 expression may improve current therapeutic strategy of HCC.

1.2 Cancer immunotherapy

Cancer immune escape is one of the hallmarks for human tumors development (34) and augmenting immune surveillance in patients with cancer has been a fundamental strategy in the development of cancer immunotherapy (13, 20, 35-37). To date, two broad approaches have been utilized to enhance the anti-tumor immune response. First, effector cells and

molecules of the immune system have been used to directly eliminate tumor cells in a process also known as “passive immunotherapy”. This approach includes antibody-targeted therapy and its derivatives (e.g., antibody-drug conjugates), and chimeric antigen receptor (CAR)-T cell/ CAR-Natural Killer (NK) cell therapy. Passive immunotherapy applies the power of modern technology and specifically targets tumor cells using molecules located on the cell surface (38, 39). Second, manipulating endogenous regulatory and/or activating processes in order to enhance the anti-immune response, also known as “active immunotherapy”, has also led to much success in recent years. Examples of such an approach include: 1) using cytokines or cancer vaccines to enhance antigen uptake, processing, and presentation to T cells by antigen presenting cells (APCs; 2) increasing the activation and expansion of naive T cells by vaccine and anti-CTLA-4 therapy; 3) intensifying the effector phase of the immune response in tumor microenvironment (13, 35, 40) using adoptive cell therapy with *ex vivo* stimulated. Currently, multiple immunotherapeutic agents have either been approved by FDA or are currently being tested in clinical trials, including IL-2 therapy, immune checkpoint blockade (ICB; anti-CTLA4, PD-1 and PD-L1 antibodies), (CAR)-T cell therapy (Kymriah and Yescarta; for targeting CD19), oncolytic virus (41) and cancer vaccines (Human papillomavirus (HPV) vaccine). Overall, these strategies focus on for boosting immune surveillance in cancer patients, and have provided profoundly clinical benefit in patients with cancer.

1.3 The biosynthesis and post-translational modification of PD-L1

PD-L1 (also known as B7 homolog 1 and CD274), is an immune checkpoint protein and its engagement with PD-1 receptor on T cells activates co-inhibitory signaling, thereby suppressing the function of cytotoxic T lymphocytes (CTLs)and allowing cancer cells to evade

immune surveillance (19, 42). Although PD-L1 or PD-1 blockade has demonstrated resulted in improved outcomes in the clinic (19, 36, 43), the mechanism of increased PD-L1 expression in tumor microenvironment is not fully understand.

Intrinsic and adaptive signaling pathway tightly control the expression of immune checkpoint molecule in tumor microenvironment (44). Several oncogenic signaling pathways upregulate PD-L1 RNA expression or maintain the stability of PD-L1 mRNA in cancer cells, including epidermal growth factor receptor (EGFR), the transcription factor MYC, KRAS, and the kinase AKT (45-48). These mechanisms have been proposed as potential cancer therapeutic targets. In addition to oncogenic signaling pathways, PD-L1 expression can also be upregulated through an adaptive signaling pathway in response to anti-tumor immune activity (44). Notably, IFN-γ secreted by infiltrating lymphocytes activates the STAT1 pathway in tumor cells, leading to increased transcription of PD-L1 RNA. In addition, IFN-γ-induced activation of the eIF4F–STAT1–PD-L1 axis also enhances the expression of PD-L1 via post-transcriptional regulation (49). Although these findings provide additional insight into potential mechanisms by which PD-L1 expression is regulated by the anti-tumor immune response, the role of oncogenic signaling pathways in suppressing the anti-tumor immune response through regulation of PD-L1 expression after protein translation remains unclear.

Recent studies on glycoprotein biosynthesis in cancer cells suggested that targeting this process could represent an effective biomarker-guided therapeutic strategy to improve response rates to immunotherapy (50-53). Notably, PD-L1 was shown to be highly glycosylated (52, 53), and N-linked glycosylation (N-glycosylation) of PD-L1 critically maintains its protein stability and is required for its interaction with PD-1 (51-53). Specifically, N-glycosylation of PD-L1 prevents its serine (Ser)/threonine (Thr) phosphorylation by

glycogen synthase kinase 3β (GSK3β) and consequently reduces subsequent recruitment of β-TrCP-induced protein degradation, thereby stabilizing PD-L1 and suppressing the activity of CTLs (52). In addition, the p65/CSN5 and CDK4/6 signaling pathways have also been reported to maintain PD-L1 stabilization by modulating its ubiquitination (54, 55). We recently further demonstrated that the endoplasmic reticulum (ER)-associated N-glycosyltransferase isoforms STT3A and STT3B, which are the catalytic subunits of the oligosaccharyltransferase complex, are critical for N-glycosylation and stabilization of PD-L1 (53). Moreover, our recent research also showed AMP-activated protein kinase (AMPK) phosphorylates newly synthesized PD-L1 within the ER lumen. This Ser phosphorylation of PD-L1 results in abnormal N-glycosylation structure on PD-L1 and triggers ER-associated degradation of PD-L1 (56). However, it is still unclear how the oncogenic pathways directly initiate PD-L1 glycosylation and enhance its immunosuppressive function in cancer cells.

1.4 Rationale

Previously, we showed that N-linked glycosylation on PD-L1 is required for maintaining PD-L1 stability and interaction with PD-1. In addition, inhibiting the PD-L1/PD-1 interaction with a glycosylation-specific antibody demonstrated significant therapeutic efficacy in cancer mouse model. However, the mechanism by which oncogenic signaling pathways initiate the glycosylation process of PD-L1 is not well understood. Based on results from an unbiased screen, we found that the IL-6/JAK1 pathway maintains PD-L1 stability in HCC cells. Because glycosylation is required for PD-L1 stability, we therefore asked whether IL-6/JAK1 pathway upregulates PD-L1 by modulating its glycosylation and hypothesize that

a combinatorial treatment approach involving anti-IL-6 and an immune checkpoint inhibitor is a potential therapeutic strategy for improving patient survival in HCC.

CHAPTER 2. MATERIAL and METHODS

2.1 Animal and toxicity studies

All animal experiments were performed in accordance with guidelines approved by the MD Anderson Institutional Animal Care and Use Committee. Male 6-to-8-week-old C57BL/6J (000664) and NSG (005557) mice were purchased from The Jackson Laboratory (Bar Harbor, ME, USA). Murine Hepa 1-6 cells (5×10^6), pGIPZ-sh(m)PD-L1/Flag-(m)PD-L1WT or Y112F Hepa 1-6 cells (5×10^6), B16F10 cells (5×10^4), or pGIPZ-sh(m)PD-L1/Flag-(m)PD-L1WT or Y112F B16F10 cells (5×10^4) in 50 μl of medium mixed with 50 μl of Matrigel basement membrane matrix (BD Biosciences) were injected subcutaneously into the right flanks of mice. IL-6 (150 μg, MP5-20F3; Bio X Cell, West Lebanon, NH, USA) and Tim-3 (150 μg, B8.2C12; Bio X Cell) antibodies and an isotype control antibody (150 μg, BE0088; Bio X Cell) were administered to mice via intraperitoneal injection following the indicated treatment protocol (Figure 12 and 18). Tumor size was measured as indicated in the figures (Figure 13,19, 47, 49 and 52), and tumor volume was calculated using the formula $1/2 \times \text{length} \times \text{width}^2$. Blood (200 μl) was collected from the orbital sinuses of mice using microhematocrit capillary tubes at the end of the experiment. Serum samples were subjected to biochemical analysis for the liver marker enzymes alanine transaminase (ALT) and aspartate transaminase (AST) and the kidney marker byproducts creatinine (CK) and blood urea nitrogen (BUN) to measure the toxicity of therapy using a COBAS INTEGRA 400 plus analyzer (Roche Diagnostics, Rotkreuz, Switzerland) in the Department of Veterinary Medicine and Surgery at MD Anderson.

2.2 Immunohistochemical staining (IHC) of human HCC samples

Paraffin-embedded HCC tissue array slides with 183 patient samples were obtained from Liver Surgery Department at Zhongshan Hospital, Fudan University (Shanghai, People's Republic of China). Immunohistochemical staining of tissue array was performed as described previously (52). Briefly, tissue samples were incubated with antibodies against IL-6 (sc-130326; Santa Cruz Biotechnology) and PD-L1 (ab205921; Abcam) and then incubated with an avidin-biotin-peroxidase complex. Visualization was performed using amino-ethylcarbazole chromogen. For statistical analysis, the Fisher exact test and Spearman rank correlation coefficient were used, and *P* values less than 0.05 were considered statistically significant. Using histologic scoring, the staining intensity was ranked into one of three groups: high (score 3), medium (score 2) and low (score 1 and 0).

2.3 Reagents

MG-132 and cyclophosphamide were purchased from Sigma-Aldrich. The following reagents were purchased from PeproTech Rocky Hill, NJ, USA): IFNγ, CCL1, IL-6, macrophage colony-stimulating factor, chemokine (C-X-C motif) ligand 9, CCL3, TNFα, TNFβ, and platelet-derived growth factor-BB. Ruxolitinib was purchased from Advanced ChemBlocks (Burlingame, CA, USA).

2.4 Plasmids and constructs

A pGIPZ dual expression construct for knockdown and re-expression of Flag PD-L1 was constructed as described previously (Li et al., 2016). Briefly, green fluorescent protein

cDNA on a pGIPZ-sh human (h) PD-L1 clone (3'-untranslated region of (h)PD-L1: TTGACTCCATCTTTCTTCA; Thermo Fisher Scientific, Pittsburgh, PA, USA) was replaced with Flag-(h)PD-L1 WT (shRNA and ORFeome Core, MD Anderson). The pGIPZ-sh(h)PD-L1/Flag-PD-L1 Y112F and ngPD-L1 (four glycosylation sites: N35, N192, N200, and N219 to Q) were generated via site-directed mutagenesis of pGIPZ-sh(h)PD-L1/Flag-PD-L1 WT. The same methods were applied for generating pGIPZ-sh mouse (m) PD-L1/Flag-(m)PD-L1 WT and Y112F plasmids using pGIPZ-sh(m)PD-L1 clone #3 (Thermo Fisher Scientific) and Flag-(m)PD-L1 WT (shRNA and ORFeome Core, MD Anderson). pPET21a His-PD-L1 was constructed by inserting the extracellular domain of PD-L1 (a.a. 19-238) into a pPET21a vector. pcDH-mycJAK1 was constructed by cloning JAK1 cDNA from 293T cells and inserting it into a pcDH vector.

2.5 Cell culture

The cell lines Hep 3B, SK-HEP-1, A375, Hepa 1-6, and B16F10 were obtained from the ATCC (Manassas, VA, USA), and HA95T/VGH (HA59T) was obtained from the Center of Molecular Medicine, China Medical University (Taichung, Taiwan). According the characteristic result from ATCC, The SK-HEP-1 cell was isolated from ascites of liver cancer patient and had been identified as being of endothelial origin. All cells were independently confirmed using short tandem repeat DNA fingerprinting at The University of Texas MD Anderson Cancer Center (Houston, TX, USA), and tests for mycoplasma infection were negative. All cell lines were cultured in Dulbecco's modified Eagle's medium supplemented with 10% fetal bovine serum and 1% antibiotic mixture. For cytokine stimulation and inhibitor-

based treatment experiments, cells were serum-starved overnight and then treated under the indicated conditions.

2.6 Generation of exogenous PD-L1 stable cells, and other knockdown (KD) and knockout (KO) stable cells

Using a pGIPZ-shPD-L1/Flag-PD-L1 dual expression construct, a lentivirus was generated, and Hep 3B, SK-HEP-1, HA59T, and A375 stable cells expressing Flag-PD-L1 WT, Y112F, or ngPD-L1 mutants with endogenous PD-L1 KD were established. The same method was employed for establishing stable murine Hepa 1-6 and B16F10 cells with Flag-PD-L1 WT or Y112F expression. JAK1-KD stable cells were generated using pLKO-JAK1 short hairpin RNA (TRCN0000295813; Sigma-Aldrich). STT3A-KO stable cells were generated using an STT3A CRISPR-Cas9 KO plasmid (sc-405155; Santa Cruz Biotechnology, Dallas, TX, USA) according to the manufacturer's instructions.

2.7 Transfection of small interfering RNA and expression vectors

Commercial small interfering RNAs were used to knock down expression of JAK1 (#1 SASI_Hs01_00174612 and #2 SASI_Hs01_00174613; Sigma-Aldrich), JAK2 (#1 SASI_Hs02_00338675 and #2 SA SASI_Hs01_00041551; Sigma-Aldrich), and TYK2 (#1 SASI_Hs01_00107854 and #2 SASI_Hs01_00107856; Sigma-Aldrich). These small interfering RNAs were transfected into Hep3B and SK-HEP-1 pGIPZ shPD-L1/Flag-PDL1 WT cells using an electroporator (Nucleofector II; Lonza, Basel, Switzerland) according to the manufacturer's instructions. pCMV HA-ubiquitin, pGIPZ shPD-L1/Flag-PDL1 WT, or Y112F

were transfected into HEK-293T cells using Lipofectamine LTX with Plus Reagent (15338100; Life Technologies, Grand Island, NY, USA).

2.8 Western blotting and co-immunoprecipitation (co-IP)

Whole-cell extracts were prepared by lysing cells in a lysis buffer containing 20 mM Tris (pH 7.5), 150 mM NaCl, 1 mM EDTA, 1 mM EGTA, 1% Triton X-100, 2 mM NaF, 1 mM Na_3VO_4, and protease inhibitor cocktail (B14002; Biotool, Houston, TX, USA) freshly added to lysis buffer before lysis. Immunoblotting was performed with primary antibodies against PD-L1 (13684, 1:1000; Cell Signaling Technology, Danvers, MA, USA), PD-L1 (GTX104763, 1:2000; GeneTex, Irvine, CA, USA), JAK1 (sc-376996, 1:1000; Santa Cruz Biotechnology), JAK1 (610231, 1:2000; BD Biosciences, San Jose, CA, USA), JAK2 (3230, 1:1000; Cell Signaling Technology), TYK2 (14193, 1:1000; Cell Signaling Technology), STT3A (sc-100796, 1:1000; Santa Cruz Biotechnology), Flag-tag (14793, 1:2000; Cell Signaling Technology), Flag-tag (F1804, 1:4000; Sigma-Aldrich), HA-tag (3724, 1:3,000; Cell Signaling Technology), phosphorylated STAT3 (Tyr705; 9145, 1:3000; Cell Signaling Technology), STAT3 (sc-482, 1:2000; Santa Cruz Biotechnology), α-tubulin (B-5-1-2, 1:5000; Sigma-Aldrich), and β-actin (A2228, 1:5000; Sigma-Aldrich). For co-IP, cells were lysed in lysis buffer. Lysates (2 mg) were mixed with antibodies against PD-L1 (13684, 1:200; Cell Signaling Technology), STT3A (sc-100796, 1:200; Santa Cruz Biotechnology), Flag-tag (14793, 1:200; Cell Signaling Technology), Flag-tag (F1804, 1:200; Sigma-Aldrich) overnight at 4°C and then pulled down using a protein G magnetic bead (161-4023, 1:10; Bio-Rad Laboratories, Hercules, CA, USA) at 4°C for 6 hr. WB signals were analyzed and quantified using the Image Studio Lite software program (LI-COR Biotechnology, Lincoln, NE, USA).

2.9 Trypsinization of endoplasmic reticulum microsomal fractions

ER microsomal fraction was collected from cells by ER enrichment kit (NBP2-29482, Novus Biologicals, Littleton, CO). After pretreatment with or without 1% Triton X-100 for 3 min, trypsin/EDTA (0.625 g/L trypsin and 0.05 g/L EDTA in PBS) solution was added to ER microsomal fraction. Samples were incubated for the indicated time. After trypsinization, samples were analyzed by Western blotting using primary antibodies against IRE1α (32941:2000; Cell Signaling Technology), HSP90B1 (NBP2-42379, 1:3000; Novus Biologicals), or JAK1 (610231, 1:2000; BD Biosciences).

2.10 Immunofluorescence staining

Cells were washed with phosphate-buffered saline (PBS) and fixed in an ice-cold acetone-methanol mixture (1:1) for 5 min. After washing in PBS three times, the cells were placed in a blocking buffer (10% normal goat serum and 1% bovine serum albumin in PBS) at room temperature for 1 hr. The cells were then stained with primary antibody against JAK1 (sc-376996, 1:50; Santa Cruz Biotechnology) or HSP90B1 (nb300-619, 1:100; Novus Biologicals, Littleton, CO, USA) with 5% normal goat serum and 0.2% bovine serum albumin in PBS at 4 °C overnight. Secondary antibody conjugated to Alexa Fluor 594 or 488 (1:3,000; Life Technologies) were used to visualize the primary antibody. Afterward, the cells were counterstained with Hoechst dye and mounted. To show the binding between JAK1 and PD-L1, cells were subjected to Duolink in situ fluorescent staining (DUO92101; Sigma-Aldrich) with anti-JAK1 (sc-376996, 1:50; Santa Cruz Biotechnology) and anti-PD-L1 (ab205921,

1:100; Abcam, San Francisco, CA, USA) primary antibodies according to the manufacturer's instruction. After the Duolink assay, cells were further subjected to anti-HSP90B1 immunofluorescence staining as described above. Fluorescent images of the cells were observed under an LSM 710 confocal microscope (Carl Zeiss, Oberkochen, Germany). For image quantification of JAK1 expression, a custom software program was designed using MATLAB to analyze image data. Images were processed with background subtraction and using a Gaussian filter with a width of 2 pixels to reduce noise. Cells were then segmented using a watershed algorithm and Otsu's thresholding method. Cytoplasmic immunofluorescence signals were calculated as the average intensities within the cytoplasmic regions. For immunofluorescent staining of mouse tumor samples, tumors were isolated from mice, embedded in optimal cutting temperature blocks, and frozen for cryostat sectioning. Cryostat sections (8 μm thick) were fixed with 4% paraformaldehyde for 15 min at room temperature. After washing in PBS, sections were incubated in a blocking solution (PBS with 3% donkey serum, 1% bovine serum albumin, 0.3% Triton X-100, pH 7.4) for 30 min at room temperature. Samples were stained with primary antibodies against CD8 (MCA609G, 1:100; Bio-Rad Laboratories) and granzyme B (AF1865, 1:500; R&D Systems, Minneapolis, MN, USA) in an antibody reaction buffer (PBS plus 1% bovine serum albumin, 0.3% Triton X-100, pH 7.4) overnight at 4 °C followed by secondary antibodies conjugated with Alexa Fluor 350, 488, 546, and 647 (1:3,000; Life Technologies) at room temperature for 1 hour. Hoechst 33342 (Life Technologies) was used for nuclear staining. Fluorescent images of the cells were observed as described above.

2.11 Quantitative real-time RT-PCR

Total RNA was extracted from cells using an RNeasy Mini Kit (QIAGEN, Valencia, CA, USA) after washing with PBS. cDNA was synthesized from purified RNA using a SuperScript III First-Strand cDNA synthesis system (18080051; Life Technologies) according to the manufacturer's instructions. Quantitative polymerase chain reaction (PCR) analysis was performed using a real-time PCR machine (iQ5; Bio-Rad Laboratories). The comparative Ct method was used for data analysis. Human PD-L1 mRNA was normalized to human actin mRNA. The primer sequences for quantitative real-time reverse transcription-PCR were as follows: human PD-L1-F, 5'-TCACTTGGTAATTCTGGGAGC-3'; human PD-L1-R, 5'-CTTTGAGTTTGTATCTTGGATGCC-3'; human actin-F, 5'-GCAAAGACCTGTACGCCAACA-3'; human actin-R, 5'-TGCATCCTGTCGGCAATG-3'.

2.12 In vitro kinase assay

Expression of the recombinant proteins His-PD-L1 WT and His-PD-L1 Y112F (extracellular domain; a.a. 19–238) was induced in *Escherichia coli* (BL21) using isopropyl β-D-1-thiogalactopyranoside, and the proteins were purified using a HisTALON Superflow Cartridge (635683; Clontech, Mountain View, CA, USA). Purified recombinant proteins were incubated with activated JAK1 kinase (SRP0335; Sigma-Aldrich) and 0.2 mM ATP in a kinase buffer (5 mM $MgCl_2$, 5 mM $MnCl_2$, 50 μM Na_3VO_4, 50 mM HEPES, pH 7.4, 5 mM DTT) at 30°C for 30 min. The kinase reaction was stopped by the addition of sodium dodecyl sulfate sample and boiling. The samples were analyzed using Western blotting.

2.13 Antibody generation and detection

An anti-PD-L1 Y112 phosphorylation antibody (anti-pY112 PD-L1) was generated against the region near the Tyr112 phosphorylation site of PD-L1. The phosphorylated synthetic peptide [C-QDAGV(pY)RCMISYGGADYKR] was used for immunization in the mice. The antibody was generated as described previously (Li et al., 2016). For detecting ngPD-L1 Y112 phosphorylation, antibodies were preincubated with cold or hot peptide for 2 h at 4°C and applied to pull-down of Y112 phosphorylation of ngPD-L1 using co-IP as described.

2.14 Flow cytometric analysis and cytotoxic T lymphocyte (CTL) profile analysis in mouse tumors

Single-cell suspensions were prepared and resuspended in a staining buffer (554656; BD Biosciences). Human tumor cells were stained with APC-PD-L1 (329707, 1:100; BioLegend, San Diego, CA, USA) according to standard protocols. To analyze CTL profiles and PD-L1 levels in mouse tumor samples, a Mouse Tumor Dissociation Kit (130-096-730; Miltenyi Biotec, Bergisch Gladbach, Germany) and gentle MACS Octo Dissociator (130-096-427; Miltenyl Biotec) were used to digest mouse tumors into single cells. After removing red blood cells and hybridizing with CD16/CD32 antibody (TruStain fcX; 101319, 1:50; BioLegend), single cells were stained for flow cytometry according to standard protocols with antibodies against the following: PE-CD45 (103105, 1:200; BioLegend), APC-CD3ε (100311, 1:100; BioLegend), APC/Cy7-CD8a (100713, 1:100; BioLegend), and APC-PD-L1 (124311, 1:100; BioLegend). For further intracellular staining, cells were fixed, permeabilized, and stained with Pacific Blue IFNγ (505817, 1:50; BioLegend), Pacific Blue Granzyme B (515407,

1:50; BioLegend), or FITC- Granzyme B (515403, 1:50; BioLegend). Stained cells were analyzed using a BD FACSCanto II cytometer (BD Biosciences). Data were processed using the FlowJo software program (Ashland, OR, USA).

2.15 CD8+ tumor-infiltrating lymphocytes (TILs) co-culture assay

Mouse Tumor Dissociation Kit (130-096-730; Miltenyl Biotec) and gentle MACS Octo Dissociator (130-096-427, Miltenyl Biotec) were applied to digest tumors from mice. Percoll gradient assay (17-5445-01, GE Healthcare) was then performed to enriched leukocytes. $CD8^+$ TILs was isolated by Mouse $CD8^+$ T Cell Isolation Kit (19853, STEMCELL Technologies, Vancouver, BC, Canada). The isolated $CD8^+$ TILs was activated by Dynabeads™ Mouse T-Activator CD3/CD28 (11456D; Thermo Fisher Scientific) for 3 days according to the manufacturer's protocol. The experiments were performed in DMEM medium with IL-2 (10 ng/mL). Cancer cells were allowed to adhere to the plates overnight and then incubated for 48 hr with activated $CD8^+$ TILs in the presence or absence of IL-6 (20 ng/ml), IgG control antibody (5 μg/ml, BE0101; Bio X Cell) or mouse PD-L1 antibody (5 μg/ml, BE0090; Bio X Cell). The ratios between cancer cells and $CD8^+$ TILs is 1:5. T cells and cell debris were removed by PBS wash, and living cancer cells were then quantified by a spectrometer at OD (570 nm) followed by crystal violet staining.

2.16 Study population

Under the IRB approval from The University of Texas MD Anderson Cancer Center, total of 103 newly diagnosed patients with pathological and/or radiological confirmed HCC

diagnosis were recruited during 2014 as part of ongoing case-control study. Blood sample were collected at time of diagnosis prior to treatment intake. Clinico-radiological-pathological features of HCC patients were retrieved from medical records. Plasma samples were shipped to perform by Rules-Based Medicine ("RBM") to test the circulating level of IL6 certified by Clinical Laboratory Improvement Amendments (CLIA). Mean value was assessed in 200 normal control group who were included in the case-control study and defined as spouses and friends of other cancers.

2.17 Statistical analysis

Statistical analyses were performed using SPSS analysis tools (IBM Corporation, Armonk, NY, USA) or the Prism software program (GraphPad Software, San Diego, CA, USA). All data were presented as means ± standard deviation (S.D.). The Mann-Whitney test was used to compare two groups. One-way and repeated-measures ANOVA were used to compare multiple groups. The log-rank (Mantel-Cox) test was used to compare mouse survival rates. *P* values less than 0.05 were considered statistically significant.

CHAPTER 3. RESULTS

3.1 The Interleukin (IL)-6/Janus kinase 1 (JAK1) pathway positively regulates PD-L1 protein stability

To identify the signaling pathways that potentially affect the glycosylation and stabilization of PD-L1 in HCC, we selected pathways based on the following three criteria: 1) cytokine levels are increased in HCC patients with poor prognosis and are able to upregulate PD-L1 protein expression because PD-L1 glycosyation affects PD-L1 protein stability; 2) downstream tyrosine (Tyr) and Ser/Thr kinases interact directly with PD-L1, particularly those for which therapeutic inhibitors are approved and whose activities are blocked by these inhibitors; and 3) activated mutations are reported in HCC (Figure 1). We intended to screen for HCC-related cytokines that may upregulate PD-L1 protein expression. To that end, we developed Hep-3B and SK-HEP-1 cancer stable cells which express exogenous PD-L1 independently of the transcriptional regulation of endogenous PD-L1 by first knocking down endogenous PD-L1 and then re-expressing Flag-tagged PD-L1 using a cDNA construct driven by an exogenous CMV promoter (Figure 2). PD-L1 expression in those cell lines, Flag-PD-L1 wild-type (WT)-Hep 3B and Flag-PD-L1 WT-SK-HEP-1 cells, was no longer regulated by the endogenous PD-L1 promoter and/or splicing events. If PD-L1 protein expression is upregulated by any cytokines in those cells, it likely occurs via posttranslational modifications.

Multiple cytokines, including interferon (IFN)γ, C-C motif chemokine ligand 1 (CCL1), Interleukin (IL)-6, macrophage colony-stimulating factor (M-CSF), chemokine (C-X-C motif) ligand 9 (CXCL9), CCL3, tumor necrosis factor (TNF)α, TNFβ, and platelet-derived growth factor-BB (PDGF-BB), are elevated in HCC patients with severe hepatitis and correlated with poor prognosis (57). Among them, IL-6 and TNFα/β markedly enhanced the levels of

exogenous PD-L1 protein expression in Flag PD-L1 WT-Hep 3B and WT-SK-HEP-1 cells (Figure 3). The TNF/p65/CSN5 pathway has been shown to enhance PD-L1 expression by upregulating deubiquitination (55). In addition to the TNF family, our present findings suggested that IL-6 also upregulates PD-L1 protein expression with an unknown mechanism. Next, we examined PD-L1–binding partners of Tyr/Ser/Thr kinases by mass spectrometry and Ingenuity Pathway Analysis (Supplemental Figure 1B) and identified two kinases, Janus kinase 1 (JAK1) and tyrosine kinase 2 (TYK2), which are directly downstream of IL-6 signaling (Figure 4).

A high percentage of genetic alternations in the Janus kinase (JAK)/signal transducer and activator of transcription (STAT) pathway (45.5%) has been reported in HCC (1, 58). Moreover, high levels of IL-6 in tumor regions are correlated with poor prognosis in advanced HCC (31). HCC patients with high plasma IL-6 levels exhibited significantly poorer overall survival (median, 8.0 *vs*. 13.9 months) compared with those with low IL-6 levels (32). This prompted us to further investigate whether PD-L1 expression is upregulated by the IL-6/JAK1 pathway as HCC harbors a relatively high percentage (~7%) of gain-of-function JAK1 mutations (58). In addition, multiple IL-6/JAK1 pathway-blocking antibodies and inhibitors, e.g., IL-6 antibody siltuximab, IL-6 receptor antibody tocilizumab, and JAK1/2 kinase inhibitor ruxolitinib, have been approved by the FDA (6, 7), which makes it easier to translate into clinical setting. Indeed, PD-L1 protein expression was increased after IL-6 stimulation and decreased after treatment with ruxolitinib in Flag-PD-L1 WT-Hep 3B and WT-SK-HEP-1 cells (Figure 5). We observed similar results in parental human Hep 3B and SK-HEP-1 (Figure 6) and mouse melanoma cells (Figure 7), suggesting that the endogenous PD-L1 is also under the same regulation. In a time-course experiment, IL-6–induced PD-L1 protein

expression peaked at 12 hours after ligand stimulation (Figure 8), which was similar to the previously reported protein half-life of PD-L1 (52). Treatment with ruxolitinib, a JAK1/2 kinase inhibitor, blocked IL-6–induced PD-L1 protein expression (Figure 8, lanes 5, 6 and 7 *vs*. 2, 3 and 4) whereas the addition of proteasome inhibitor MG132 restored PD-L1 expression (Figure 9, lane 4 *vs.* 5). Moreover, knocking down JAK1 but not TYK2 reduced PD-L1 protein expression (Figure 10). Taken together, these data suggested that the IL-6/JAK1 pathway upregulates PD-L1 expression and maintains PD-L1 protein stability in HCC cells likely through the proteasome pathway.

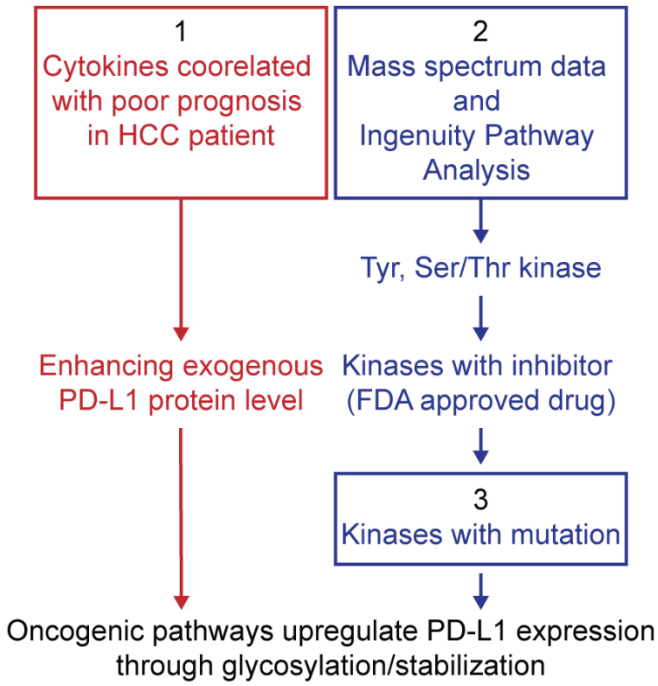

Figure 1. Strategy for identifying oncogenic pathway involved in PD-L1 post-translational modification and glycosylation.

Schematic of the strategy using the indicated criteria (1, 2, and 3) to identify pathways that potentially upregulate PD-L1 expression via posttranslational modifications.

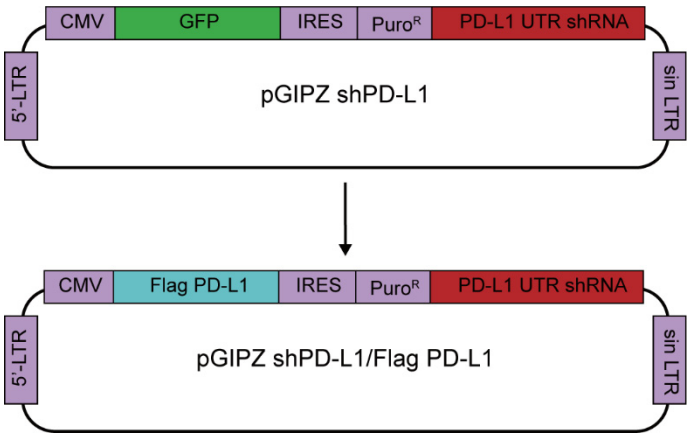

Figure 2. Map of dual expression pGIPZ constructs

Dual expression pGIPZ constructs were used to generate stable cell lines. pGIPZ vectors containing a short hairpin RNA sequence targeting the 3'-untranslated region of human or murine PD-L1 were used as templates. The original green fluorescent protein cDNA was replaced with cDNA from Flag-PD-L1 WT, Y112F, or ngPD-L1 (four glycosylation sites: N35, N192, N200, and N219 to Q).

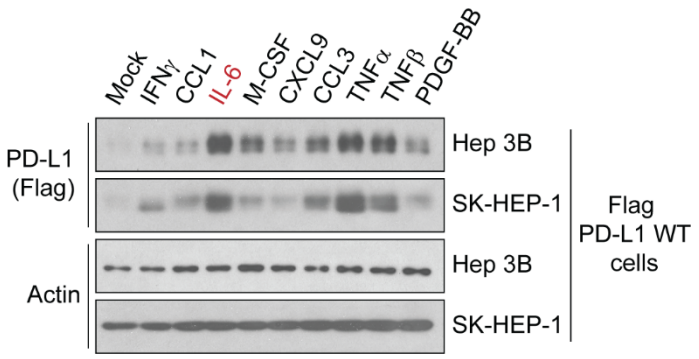

Figure 3. Cytokines upregulate PD-L1 protein level.

WB analysis of exogenous PD-L1 expression in Flag-PD-L1 WT-Hep 3B and WT-SK-HEP-1 cells stimulated with different cytokines for 18 hours.

A.

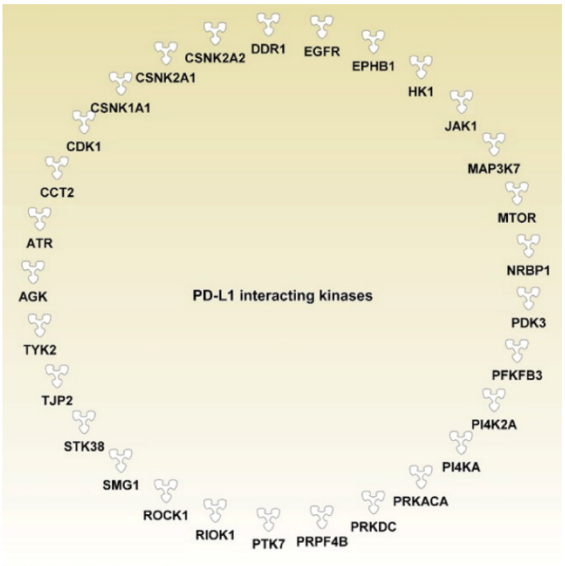

B.

PD-L1 associated Tyr/Ser/Thr kinases (with FDA-approved or commercial inhibitors)			
Tyr kinase			
JAK1	TYK2	DDR1	EGFR
Ser/Thr kinase			
TAK1	MTOR	PDK3	PRKACA
PRKDC	ROCK1	SMG1	ATR
CDK1	CSNK1A1	CSNK2A1	CSNK2A2

Figure 4. PD-L1 associated Tyr/Ser/Thr kinases and which can be targeted by available inhibitors

(A) Flag PD-L1 was immunoprecipitated from stable cells using a Flag M2 bead, purified via gel elution after electrophoresis, and subjected to liquid chromatography-tandem mass spectrometric analysis to identify PD-L1 associated partners. The binding proteins were examined using Ingenuity Pathway Analysis to identify Tyr and Ser/Thr kinases. (B) Potential PD-L1–associated kinases that can be targeted by U.S. FDA-approved or commercially available inhibitors.

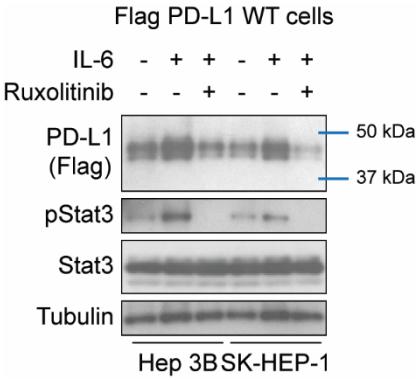

Figure 5. IL-6/JAK pathway upregulates PD-L1 protein level in HCC cancer cells.

WB analysis of exogenous PD-L1 expression in Flag-PD-L1 WT-Hep 3B and WT-SK-HEP-1 cells under IL-6 stimulation (20 ng/ml) or co-treatment with the JAK1/2 inhibitor ruxolitinib (10 μmol/L) for 18 h.

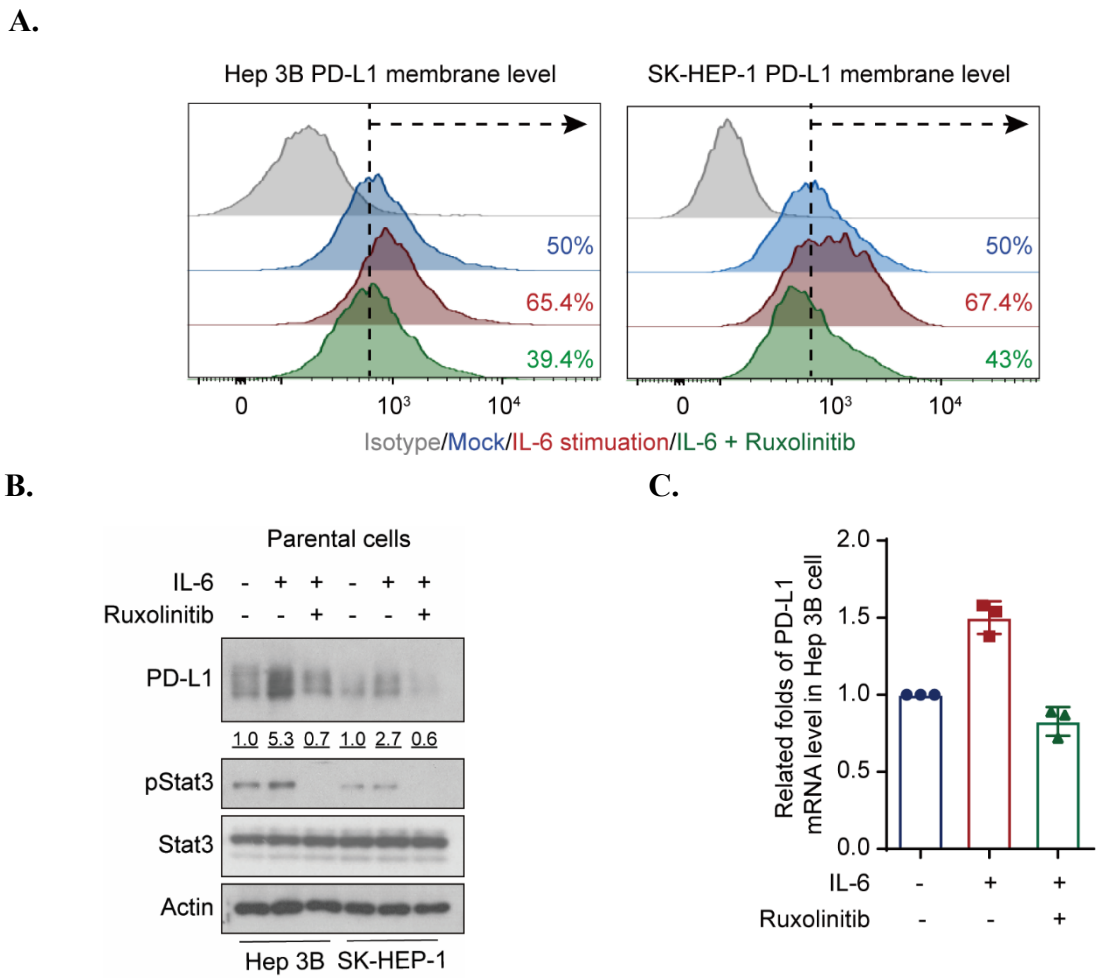

Figure 6. IL-6/JAK pathway upregulates endogenous PD-L1 in HCC cancer cells.

Flow cytometric (A), Western blot (B), and quantitative RT-PCR (C) analyses of PD-L1 expression in parental Hep 3B and SK-HEP-1 cells with or without exposure to IL-6 (20 ng/ml) and/or ruxolitinib (10 μmol/l) for 18 h. Fold increase in PD-L1 protein expression level after the indicated treatment in Hep 3B or SK-HEP-1 cells (control set to 1) are shown below the blot. Three independent experiments were performed for RT-PCR. Error bars, mean ± S.D.

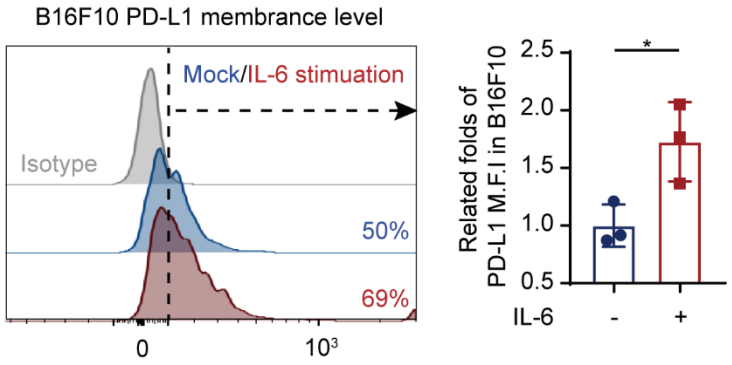

Figure 7. IL-6/JAK pathway upregulates endogenous PD-L1 protein level in mouse melanoma cells.

Flow cytometric analysis of PD-L1 expression in parental B16F10 cells with or without exposure to mouse IL-6 (25 ng/ml) for 18 h. The relative fold-change in the mean fluorescence intensity (M.F.I.) of PD-L1 is shown. Error bars represent ± S.D. *$P < 0.05$. Mann-Whitney test.

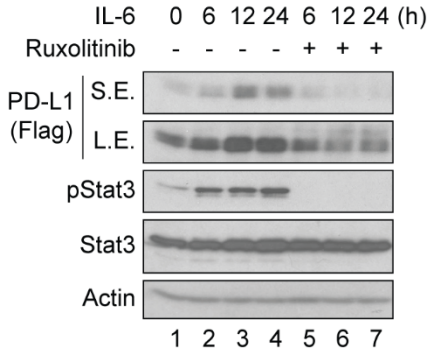

Figure 8. IL-6–induced PD-L1 protein expression peaked at 12 hours after ligand stimulation.

WB analysis of exogenous PD-L1 expression in Flag-PD-L1 WT-Hep 3B cells with IL-6 stimulation (20 ng/ml) or co-treatment with ruxolitinib (10 μmol/L) for the indicated time.

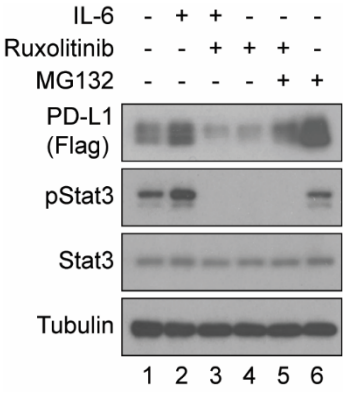

Figure 9. Proteasome degradation is involved in IL-6-induced PD-L1 protein upregulation.

WB analysis of exogenous PD-L1 expression in the presence or absence of IL-6 stimulation (20 ng/ml, 18 h), ruxolitinib (10 μmol/L, 18 h), or the proteasome inhibitor MG132 (10 μmol/L, 6 h).

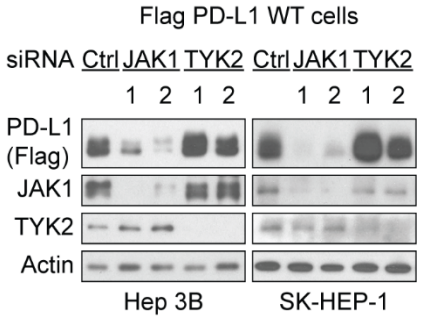

Figure 10. JAK1 is required for PD-L1 protein stability.

WB analysis of exogenous PD-L1 expression in Flag PD-L1 WT- SK-HEP-1 and WT-Hep 3B cells with knockdown of the indicated genes by small interfering RNA.

3.2 IL-6 and PD-L1 expression is positively correlated in tumor tissues from HCC patients and high IL-6 plasma level is associated with poor prognosis

To further validate the IL-6 and PD-L1 relationship in human HCC tumors, we analyzed the correlation between IL-6 and PD-L1 expression in 183 HCC patient tumor tissues. As expected, patients with high IL-6 expression also had elevated PD-L1 expression in tumors (Figure 11). Specifically, about 79% of tumor samples with high IL-6 expression exhibited strong PD-L1 staining, and 49% of those with low IL-6 expression exhibited weak or no PD-L1 staining. These result suggested that IL-6 is physiologically significant and clinically relevant to PD-L1 expression in HCC.

Previously, Shao et al. reported that high IL-6 level is associated with poorer prognosis of HCC patients (32). To further determine the clinical relevance IL-6 level and prognosis of HCC patients, we analyzed the plasma level of IL-6, clinicopathological features, and survival in 104 HCC patients from different cohort (Table 1). On the basis of this clinical cohort, we used the median value of IL-6 plasma level from control group (6 pg/ml) as a cutoff value to determine those with normal or low value versus those with high value in HCC patient cases. These results were the similar to that of previous studies (32, 59) in which the advanced HCC staging and shorter median survival months (6.4 *vs*. 19.7 months) were observed in the cohort of HCC patients with high IL-6 plasma level. Together with results from prior studies, the current findings indicated that high IL-6 level in plasma/serum is correlated with poor prognosis of HCC patients, and that IL-6 expression is positively correlated with PD-L1 expression at tumor region in HCC patients.

		Expression of IL-6			
		-/+	++	+++	Total
PD-L1	-/+	49 (89.1%)	19 (29.2%)	1 (1.6%)	69 (37.7%)
	++	6 (10.9%)	34 (52.3%)	12 (19.0%)	52 (28.4%)
	+++	0 (0.0%)	12 (18.5%)	50 (79.4%)	62 (33.9%)
Total		55 (100%)	65 (100%)	63 (100%)	183 (100%)

P value, p=0.0001

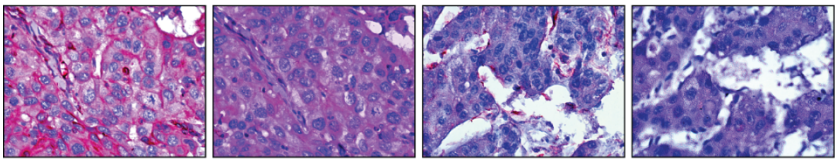

IL-6 PD-L1 IL-6 PD-L1

Case 1 Case 2

Figure 11. High IL-6 expression also had elevated PD-L1 expression in HCC tumor samples.

Correlations between expression levels of IL-6 and PD-L1 in surgical specimens of HCC analyzed using the PASS Pearson chi-square test. Representative images of IL-6 and PD-L1 expression levels in tumor regions in HCC patients.

Variable	Low Values	High Values	P value
	N= 60 (%)	N= 43 (%)	
Sex			0.1
Male	39 (65%)	33 (76.7%)	
Females	21 (35%)	10 (23.3%)	
Hepatitis (HCV/HBV)			0.1
Positive	29 (48.3%)	26 (60.5)	
Negative	31 (51.7)	17 (39.5)	
Cirrhosis			0.1
Presence	32 (53.3%)	29 (67.4)	
Absence	28 (46.7%)	14 (32.6%)	
Child-Pugh			0.006
A	8 (13.3%)	4 (9.3%)	
B	48 (80%)	26 (60.5%)	
C	4 (6.7%)	13 (30.2%)	
TNM Staging			
I_II	25 (49%)	10 (23.8%)	0.03
III-A-III-B	12 (23.5%)	19 (45.2%)	
III-C-IVB	14 (27.5%)	13 (31%)	
BCLC Staging			0.02
0-B	14 (24.6%)	3 (7%)	
CD	43 (75.4%)	40 (93%)	
CLIP Staging			0.0001
0-2	37 (72.5%)	14 (33.3%)	
3	10 (19.6%)	13 (31%)	
4-6	4 (7.8%)	15 (35.7%)	
Median Survival (95% CI) months	19.7 (15-5-23.8)	6.4 (1-16.5)	0.04

Table 1. Correlation between IL-6 plasma level and staging in HCC patients.

Associations between plasma IL-6 levels and HCC patient characteristics and median survival months

3.3 Blocking IL-6/JAK1-mediated PD-L1 protein stability enhances the efficacy of anti-T-cell immunoglobulin mucin-3 (Tim-3) immunotherapy

Because blocking IL-6/JAK1 pathway abolished PD-L1 stability *in vitro* and IL-6 expression is positively correlated with of PD-L1 expression in human HCC tumor tissues and poorer prognosis of HCC patients, we next asked whether neutralization of IL-6, which blocks IL-6/JAK1 pathway, downregulates PD-L1 expression and functionally mimics anti-PD-1/PD-L1 effects to reduce HCC tumorigenesis *in vivo*. In addition, previous studies have also shown that combined blockade of immune checkpoints was more effective in reversing T cell exhaustion and restoring anti-tumor immunity than single agent treatment (19, 36, 43, 53). Co-expression of Tim-3 and PD-1 on tumor-infiltrating lymphocytes has been as an indicator of T cell exhaustion, including CD8 T cells, in the HCC and other cancers tumor microenvironment (17, 60). We further asked whether combining IL-6 antibody with other immune checkpoint therapies can enhance the therapeutic efficacy. We examined the effects of anti-IL-6 and anti-Tim-3 combination therapy in a Hepa 1-6 liver cancer immunocompetent mouse model (Figure 12), which has been used in multiple cancer immunotherapy researches (61). Notably, combining IL-6 and Tim-3 antibodies reduced tumor growth and increased response rates much more significantly than did each treatment alone in immunocompetent mice bearing Hepa 1-6 tumors (Figure 13) without causing significant changes in kidney or liver function or body weights (Figure 14). As expected, treatment with the IL-6 antibody decreased PD-L1 expression levels in the tumor regions (Figure 15). Of note, the regression of tumor growth was detected in combination treatment group and tumors were eradicated in 30% of mice (3/10) in that group in 3 treatment cycles (indicated by arrows in Figure 12 combined group). Notably, no tumor recurrence was observed in these mice with complete response over 8 months (data not shown). The combination of anti-IL-6 and anti-Tim-3 not only downregulated PD-L1 but

also markedly increased the population of granzyme B and IFNγ-positive CD8 T cells in the tumor region (Figure 16). Importantly, we observed significantly improved overall survival rate compared with either antibody alone with only 3 treatment cycles (Figure 17). Similar results were observed in a more aggressive B16F10 melanoma model (Figure 18 to 20). These results indicated that blocking the IL-6 pathway downregulates PD-L1 expression and enhances efficacy of anti-Tim-3 immunotherapy.

A.

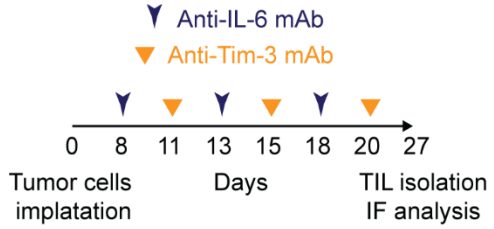

B.

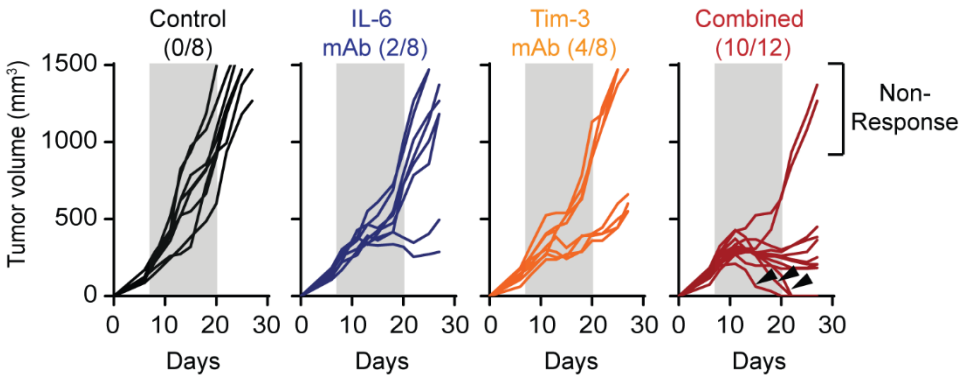

Figure 12. Anti-IL-6 and Tim-3 monoclonal antibody combined therapy in Hepa 1-6 tumor bearing mice

(A) Schematic of the treatment schedule for the IL-6 and Tim-3 monoclonal antibody (mAb) combination therapy. (B) Growth of Hepa 1-6 tumors in mice treated with the IL-6 monoclonal antibody (mAb), Tim-3 mAb, or the combination. The number of mice that experienced tumor progression in each group is shown in parentheses. The gray box in each panel indicates the duration of treatment

A.

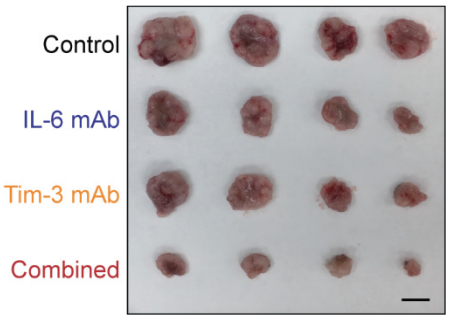

B.

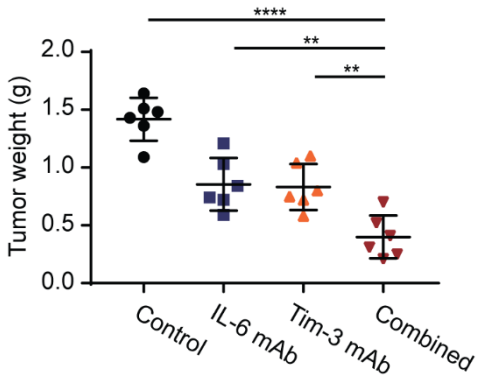

Figure 13. Size and weight of tumors from indicated treatments in Hepa 1-6 tumor bearing mice.

(A) Representative images showing tumor harvested from mice bearing Hepa1-6 tumors administered IL-6 mAb, Tim-3 mAb, or the combination. (B) Weight of Hepa 1-6 tumors in mice given an IL-6 mAb, Tim-3 mAb, or both ($n = 6$). Error bars represent ± S.D. $^{**}P < 0.01$; $^{****}P < 0.0001$. one-way ANOVA.

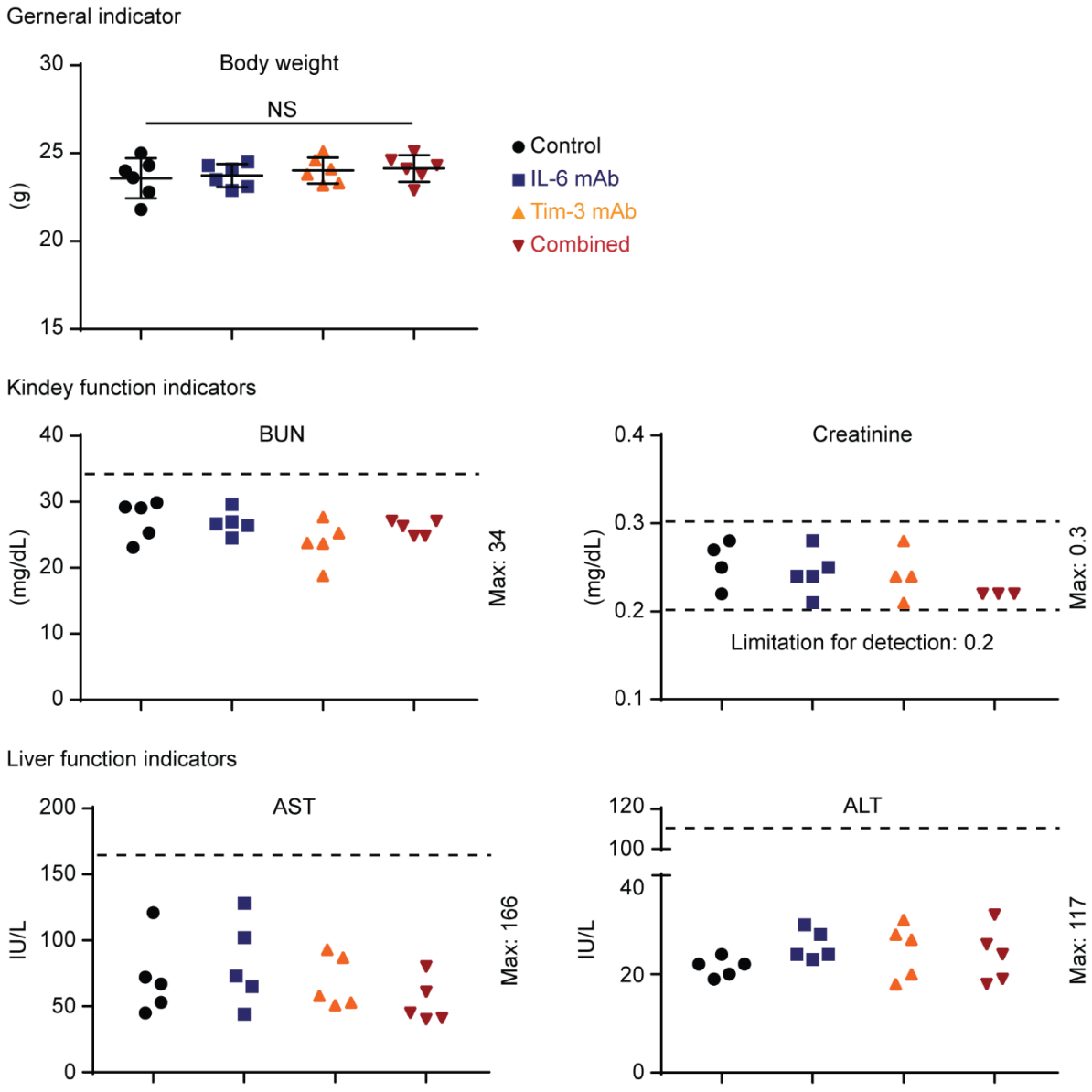

Figure 14. ***In vivo*** **toxicity detection.**

Body weight, and kidney and liver function indicators in Hepa 1-6 tumor-bearing mice (n = 5) after each indicated treatment. Maximum and normal ranges are indicated by the dashed lines. Error bar, mean ± S.D. NS, not significant.

A.

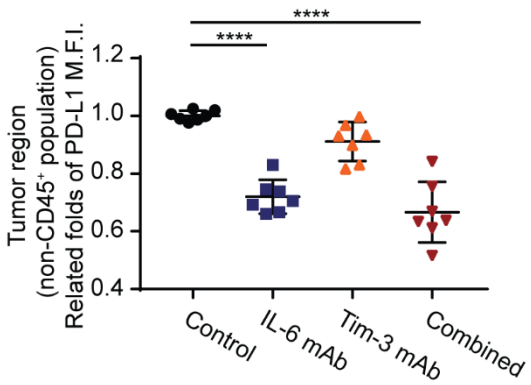

B.

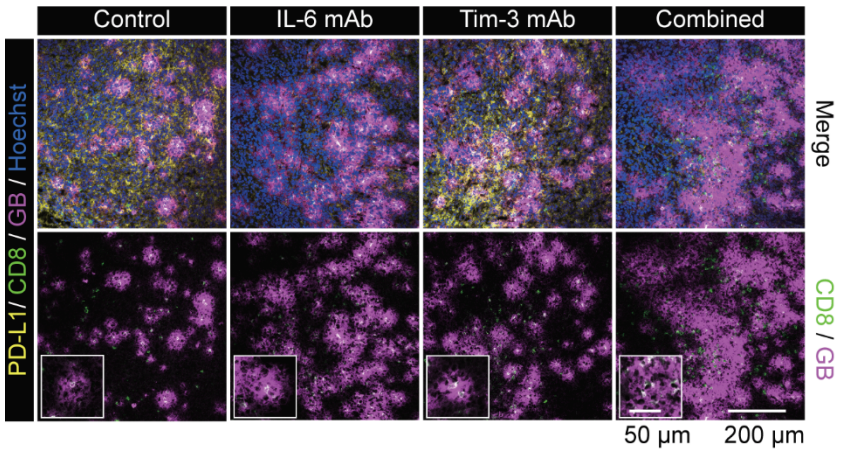

Figure 15. PD-L1 level is decreased in tumor region under IL-6 blockade condition.

(A) Flow cytometric analysis of cell surface PD-L1 expression in Hepa 1-6 tumor region (non-$CD45^+$ population) treated with the indicated regimens ($n = 7$). The relative fold-change in the M.F.I. of PD-L1 is shown. (B) Representative images of immunofluorescence staining for PD-L1, CD8, and granzyme B (GB) expressions in tumor regions in mice administered the indicated treatment. Magnified images showing co-localization of CD8 and granzyme B signals. Error bars represent ± S.D. ****$P < 0.0001$. one-way ANOVA.

A.

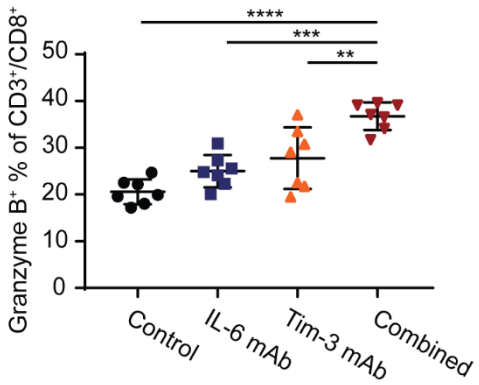

B.

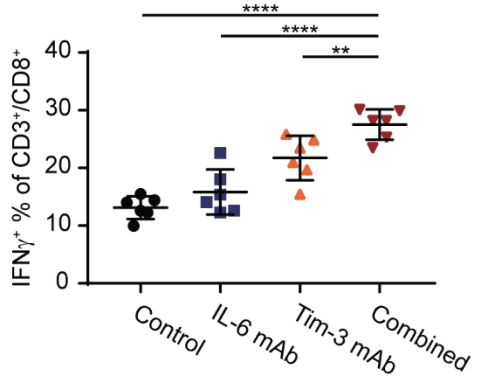

Figure 16. Population of activated cytotoxic CD8$^+$ T cell is increased in tumor microenvironment from tumor bearing mice with combined therapy.

(A) The percentage of granzyme B-positive CD3$^+$/CD8$^+$ T cells in Hepa 1-6 tumors with the indicated treatments according to flow cytometry analysis (n = 7). (B) Percentage of IFNγ-positive CD3$^+$/CD8$^+$ T cells in tumor samples obtained from Hepa 1-6 tumor-bearing mice administered the indicated treatments (n = 6). Error bars represent ± S.D. **P < 0.01; ***P < 0.001; ****P < 0.0001. one-way ANOVA**.**

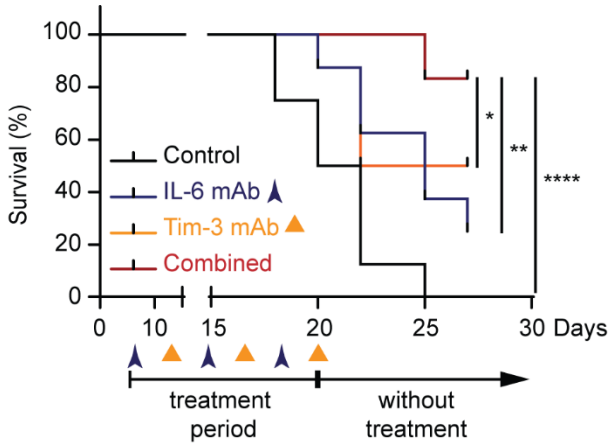

Figure 17. Anti-IL-6 and Tim-3 antibodies combined therapy improve Hepa 1-6 tumor bearing mice survival rate.

Survival curves for the data in Figure 12. *P <. 0.05; ***P < 0.001; ****P < 0.0001. log-rank [Mantel-Cox] test.

A.

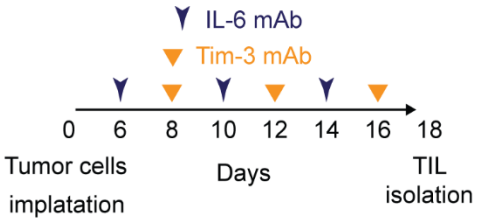

B.

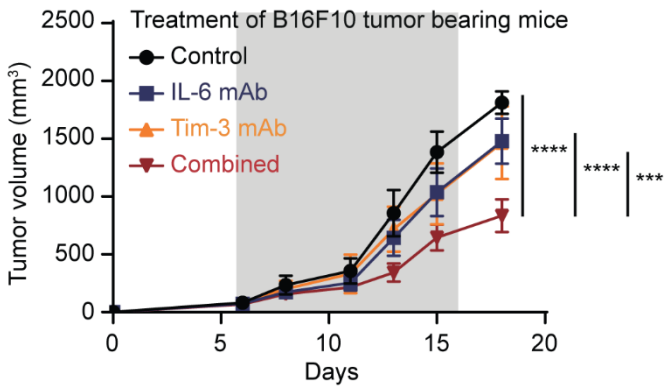

Figure 18. Anti-IL-6 and Tim-3 antibodies combined therapy reduce tumorigenesis in B16F10 tumor bearing mice.

(A) Schematic of the treatment schedule for the combination of IL-6 and Tim-3 mAbs in B16F10 tumor bearing mice. (B) Tumor growth in mice bearing B16F10 tumors were administered IL-6 mAb, Tim-3 mAb, or the combination (n = 8). The gray box in each panel indicates the duration of treatment. Error bars, mean ± S.D. ***P < 0.001; ****P < 0.001, repeated-measures ANOVA.

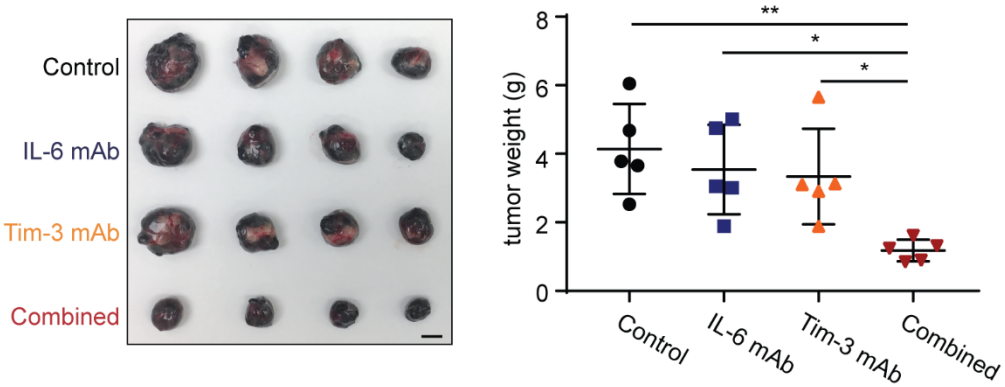

Figure 19. Size and weight of tumors from indicated treatments in B16F10 tumor bearing mice.

Tumor size and weight (n = 5) of mice administered the indicated treatment. Error bars, mean ± S.D. *P < 0.05;**P < 0.01, one-way ANOVA.

A.

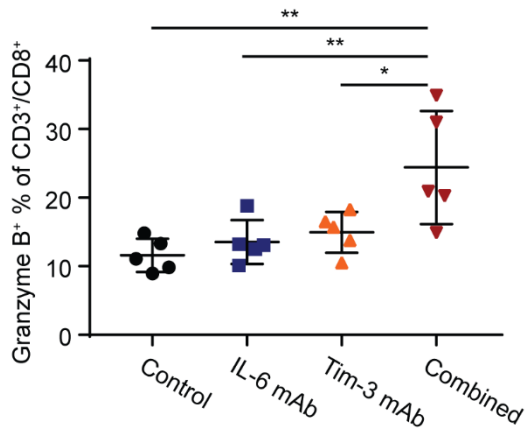

B.

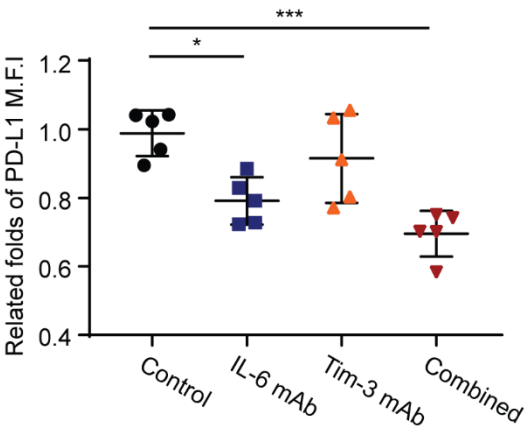

Figure 20. Anti-IL-6 and Tim-3 antibodies combined therapy enhances immune surveillance in B16F10 tumor microenvironment.

(A) Flow cytometric analysis of granzyme B-positive $CD3^+/CD8^+$ T cells in B16F10 tumors subjected to the indicated treatments (n = 5). (B) Flow cytometric analysis of the cell surface expression of PD-L1 from B16F10 tumors subjected to the indicated treatment (n = 5). Error bars, mean ± S.D. *P < 0.05;**P < 0.01; ***P < 0.001, one-way ANOVA.

3.4 IL-6/JAK1 pathway upregulates PD-L1 expression by enhancing its association with N-glycosyltransferase STT3A

Encouraged by the downregulation of PD-L1 expression via neutralization of IL-6 and the impressive therapeutic efficacy from the combination of anti-IL6 and anti-Tim3 therapy *in vivo*, we sought to investigate the detailed molecular mechanisms. To this end, we first asked whether glycosylation is involved in IL-6/JAK1-mediated PD-L1 stabilization since N-glycosylation maintains protein stability of PD-L1 (51, 52). We used a mutant PD-L1 in which four glycosylation sites (N35, N192, N200, and N219) on its extracellular domain are mutated to mimic the non-glycosylated form (ngPD-L1) (51, 52) (Figure 21). Under IL-6 stimulation, PD-L1 WT protein expression was increased, but the increase was attenuated by the addition of ruxolitinib in Flag-PD-L1 WT-Hep 3B and WT-SK-HEP-1 cells (Figure 21, lanes 1–3). As expected, ngPD-L1 expression was not affected by IL-6 or ruxolitinib (Figure 21, lanes 4–6). Similar results were observed in Flag-PD-L1 WT-PD-L1 and ngPD-L1 melanoma cells with the same treatment (Figure 22). These results suggested that glycosylation is required for the IL-6/JAK1 pathway-enhanced PD-L1 protein stability in cancer cells.

To further explore the mechanism underlying IL-6/JAK1 pathway-mediated upregulation of PD-L1 expression via glycosylation, we searched for N-glycosyltransferases that may interact with PD-L1. Among the 15 N-glycosyltransferases identified as PD-L1-associated proteins (51), seven are components of oligosaccharyltransferase complex and located in the endoplasmic reticulum (ER; Table 2). STT3 isoforms, the catalytic subunits of the oligosaccharyltransferase complex, are essential for PD-L1 glycosylation and protein stabilization (53). Therefore, we compared the complex forming ability of PD-L1 with the STT3 isoforms. We found that STT3A associated with ngPD-L1 much stronger than did WT PD-L1 by co-immunoprecipitation (co-IP; Figure 23). Knocking out STT3A also blocked IL-

6/JAK1-induced PD-L1 expression in HCC and melanoma cells (Figure 24 and Figure 25). Of note, IL-6 enhanced the complex forming ability of JAK1 and STT3A with ngPD-L1 and increased ngPD-L1 Tyr phosphorylation (4G10), which were attenuated by ruxolitinib treatment (Figure 26, lane 2 *vs*. 1 and 3). Activated JAK1 directly phosphorylated ngPD-L1 (please see later in Figure 33). These results suggested that IL-6 modulates PD-L1 glycosylation initiation by enhancing JAK1/ngPD-L1 association, JAK1-driven Tyr phosphorylation, and STT3A recruitment.

Because glycosylation initiation mainly occurs in the ER and JAK1 interacts with ngPD-L1, we further examined the localization of their interaction. Using commercially available JAK1 (Figure 27) and PD-L1 (Ab205921; specifically recognizes the extracellular domain of PD-L1) antibodies, we detected co-localization of PD-L1/JAK1 interaction in the ER with an ER marker, HSP90B1, by Duolink assay (Figure 28). During protein glycosylation in the ER, the glycosylated region of PD-L1 (extracellular domain of PD-L1) is exposed to the ER lumen (Figure 29) (62). To further confirm whether JAK1 resides in the ER lumen, we explored an approach recently developed to validate the localization of a kinase in the ER (30). In brief, we used trypsin to digest the ER fractions with or without pre-permeabilization and then measured the protein levels of JAK1, ER transmembrane protein IRE1α (cytosolic part), and ER lumen protein HSP90B1, using the indicated antibodies (illustrated in Figure 30) (56). In the non-permeable fraction (group 2), signals for the cytosolic domain of IRE1α were rapidly reduced after trypsinization, but the protein levels of JAK1 and HSP90B1 were maintained in two different cancer cell lines (Figure 30 and 31, Triton X-100 (-)). However, in the permeable fraction (group 3), no signals of cytosolic and luminal proteins were detected after trypsinization (31 and 32, Triton X-100 (+)). These results strongly suggested localization

of JAK1 inside the ER lumen. Together, these findings suggested that the JAK1/PD-L1 interaction occurs inside the ER lumen and supported the notion that JAK1 is involved in PD-L1 glycosylation in the ER.

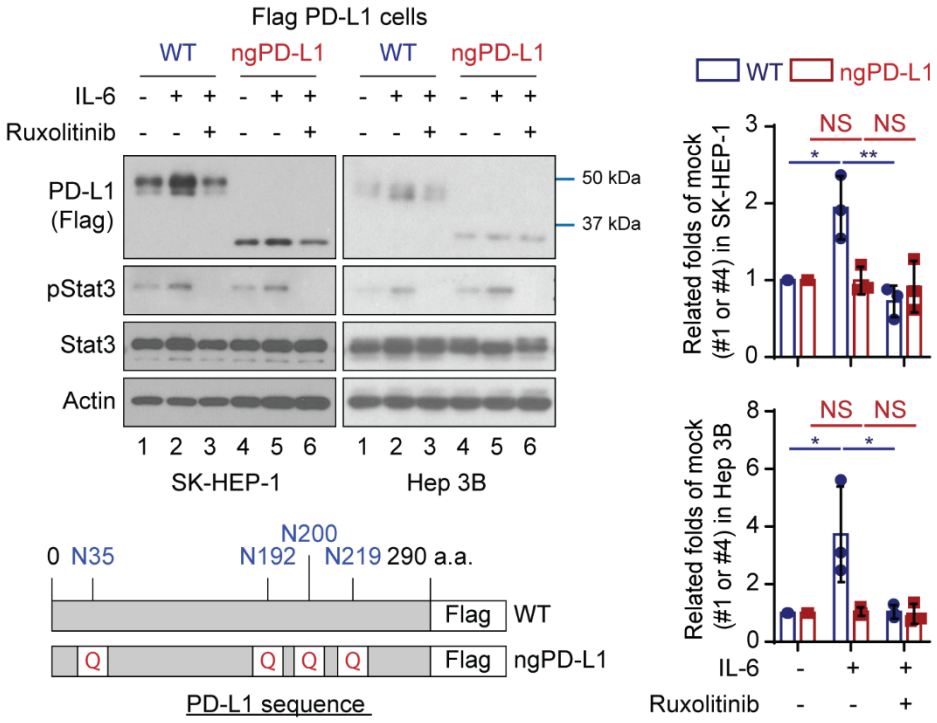

Figure 21. IL-6 enhance PD-L1 protein stability via glycosylation in HCC cells.

WB analysis of exogenous PD-L1 expression in Flag-PD-L1 WT or non-glycosylated PD-L1 (ngPD-L1) Hep 3B or SK-HEP-1 cells with or without exposure to IL-6 (20 ng/ml) and/or ruxolitinib (10 μmol/L) for 18 h. Schematic diagram of ngPD-L1 mutants used in this study. The numbers indicate amino acid positions on the PD-L1.

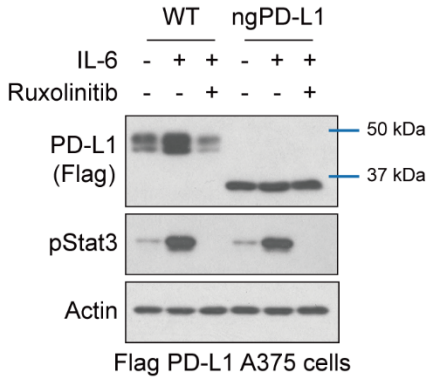

Figure 22. IL-6 enhance PD-L1 protein stability via glycosylation in melanoma cells.

WB analysis of exogenous PD-L1 expression in WT and ngPD-L1 A375 cells with or without exposure to IL-6 (20 ng/ml) and/or ruxolitinib (10 μmol/L) for 18 h.

Name	Localization	Other
PGM3	cytosol	
B3GNT3	golgi apparatus	
TMEM165	golgi apparatus	
VCP	nucleus, cytosol and ER	
KRTCAP2	plasma membrane or ER	
MOGS	ER	
ALG8	ER	
DPAGT1	ER	
STT3A	ER	Oligosaccharyl-transferase complex
STT3B	ER	
DDOST	ER	
DAD1	ER	
MGAT4B	ER	
RPN1	ER	
RPN2	ER	

Table 2. Candidates of PD-L1-interacted N-glycosyltransferases.

Candidates were described previously (51) and cataloged via their localization from http://www.genecards.org/information. Oligosaccharyl-transferase complex members are labeled as red.

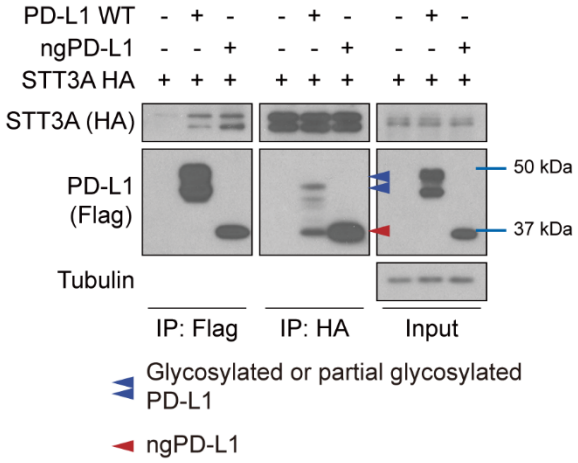

Figure 23. STT3A associated with ngPD-L1 much stronger than did WT PD-L1

Immunoprecipitation (IP) followed by WB analysis of STT3A or PD-L1 level in indicated plasms transfected Hep3B cells.

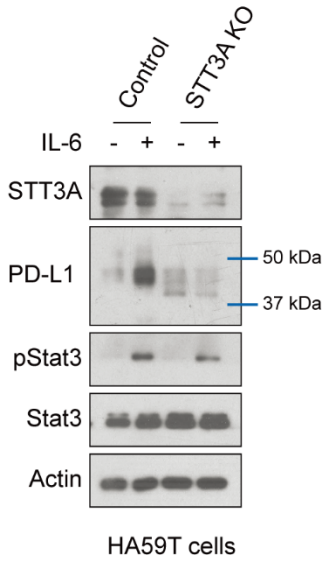

Figure 24. STT3A is required for IL-6-induced PD-L1 upregulation in HCC cells.

WB analysis of PD-L1 expression in HA59T control or STT3A knockout (KO) cells with or without IL-6 stimulation (20 ng/ml, 18 h).

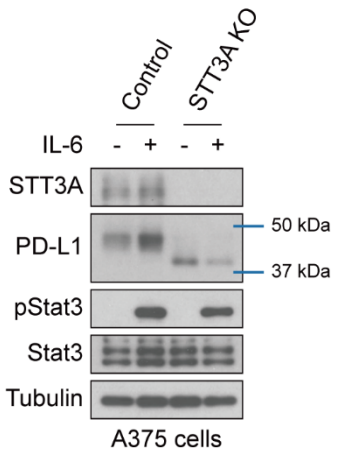

Figure 25. STT3A is required for IL-6-induced PD-L1 upregulation in melanoma cells.

WB analysis of the indicated proteins in control and STT3A knockout A375 cells with or without exposure to IL-6 (20 ng/ml) for 18 h.

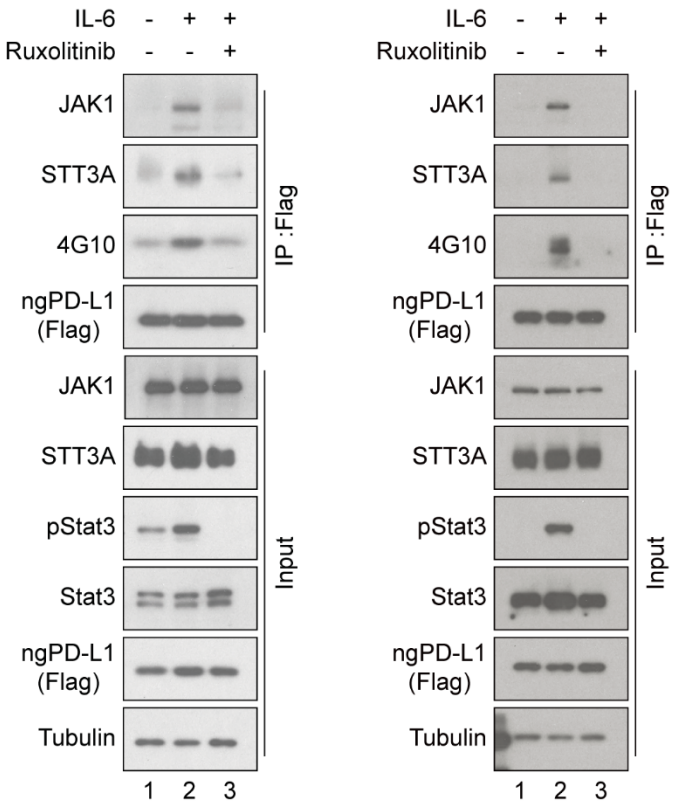

Figure 26. IL-6 enhances JAK1 and STT3A interact with ngPD-L1 and increases Tyr phosphorylation of ngPD-L1.

IP followed by WB analysis of JAK1, STT3A, and ngPD-L1 tyrosine phosphorylation (4G10) in Flag-ngPD-L1-SK-HEP-1 or Hep 3B cells with or without exposure to IL-6 (20 ng/ml) and ruxolitinib (10 μmol/L) for 30 min.

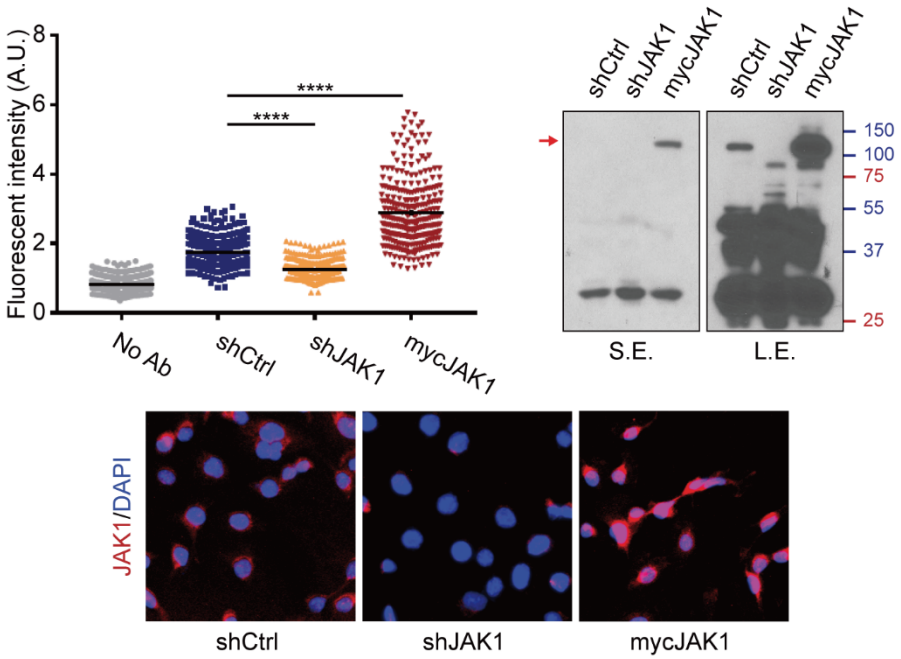

Figure 27. Characterization of the JAK1 antibody for immunofluorescence staining.

Hep 3B control short hairpin RNA (shCtrl), JAK1 knockdown short hairpin RNA (shJAK1), and JAK1 overexpressing (mycJAK1) cells were subjected to immunofluorescence staining and Western blot analysis with JAK1 antibody (sc-376996). Quantitation of immunofluorescence staining are described in Materials and Methods. S.E., short exposure; L.E., long exposure. Bars represent means. ****$P < 0.0001$, one-way ANOVA.

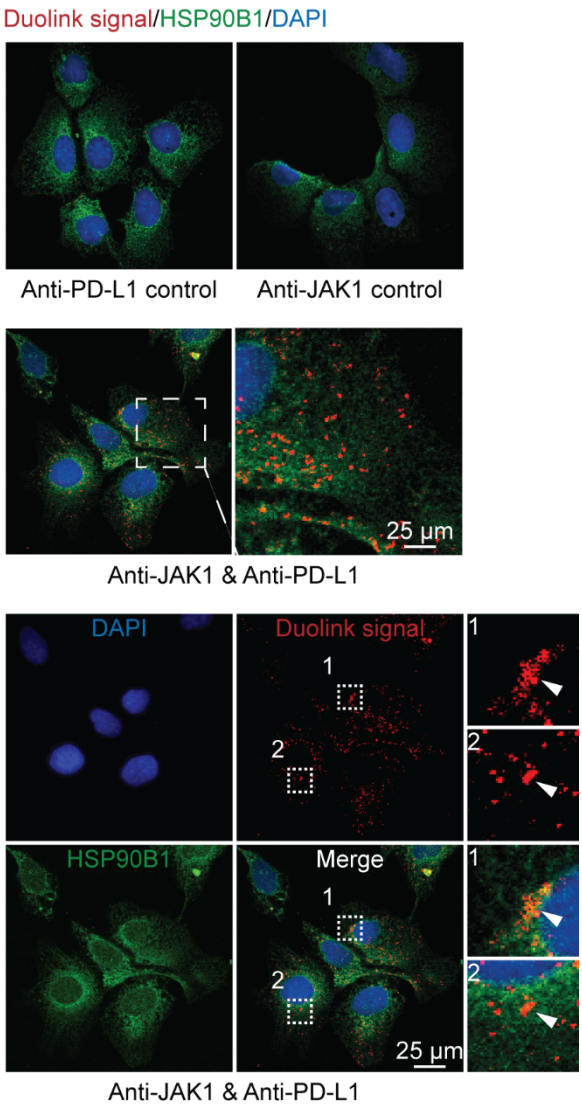

Figure 28. Interaction of JAK1 and PD-L1 in ER region.

Duolink assay of JAK1 and PD-L1 interaction in Hep 3B cells. The red dots indicate locations of their interaction. Green fluorescence (HSP90B1) was used as ER marker, and DAPI as a nuclear marker.

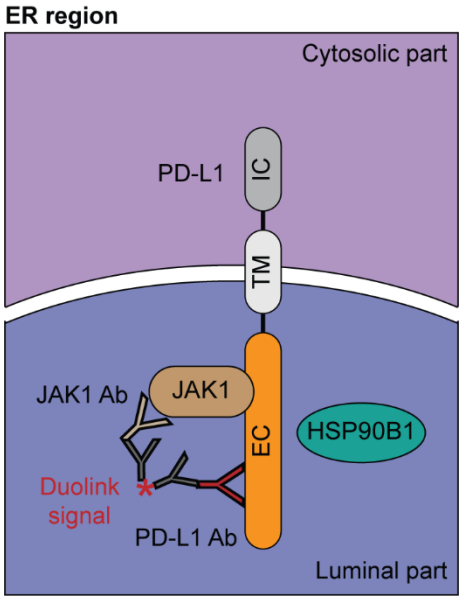

Figure 29. Schematic showing JAK1/PD-L1 interaction in the ER.

Model for showing JAK1 interact with PD-L1 extracellular domain. (IC: intracellular domain, TM: transmembrane domain, EC: extracellular domain)

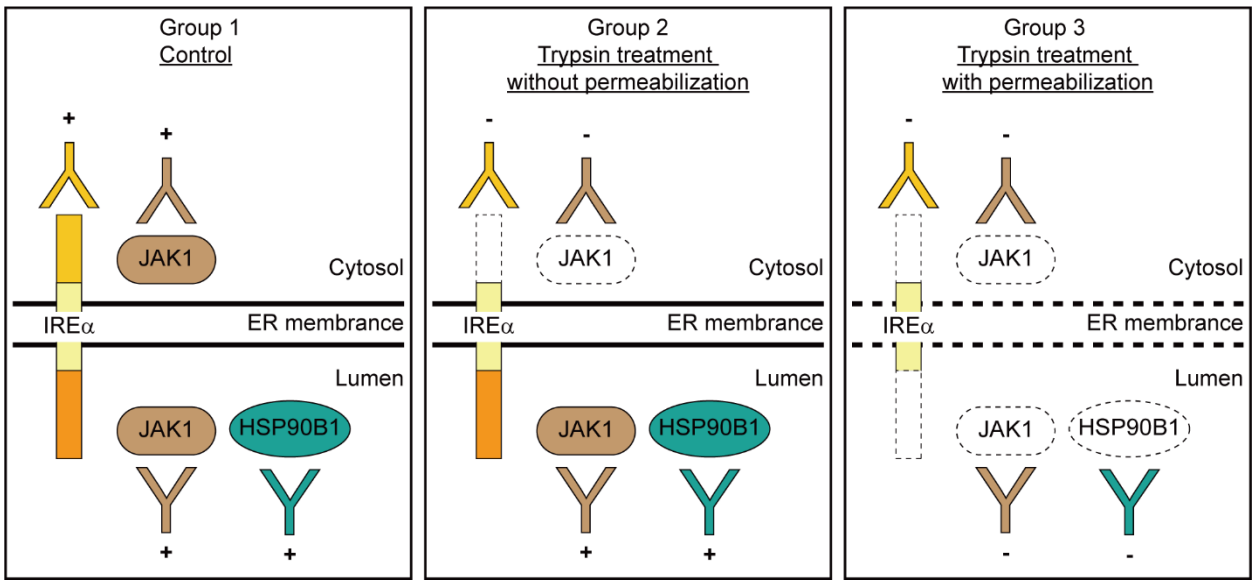

Figure 30. Model illustrating trypsinization of the ER fractions.

ER fraction without trypsin. All markers can be detected (group 1). ER fraction subjected to trypsin digestion without permeabilization. Cytosolic portions of ER proteins were not detected after digestion whereas luminal portions of ER proteins were detected (group 2). ER fraction subjected to trypsin digestion with permeabilization (1% Triton X-100). No markers were detected (group 3).

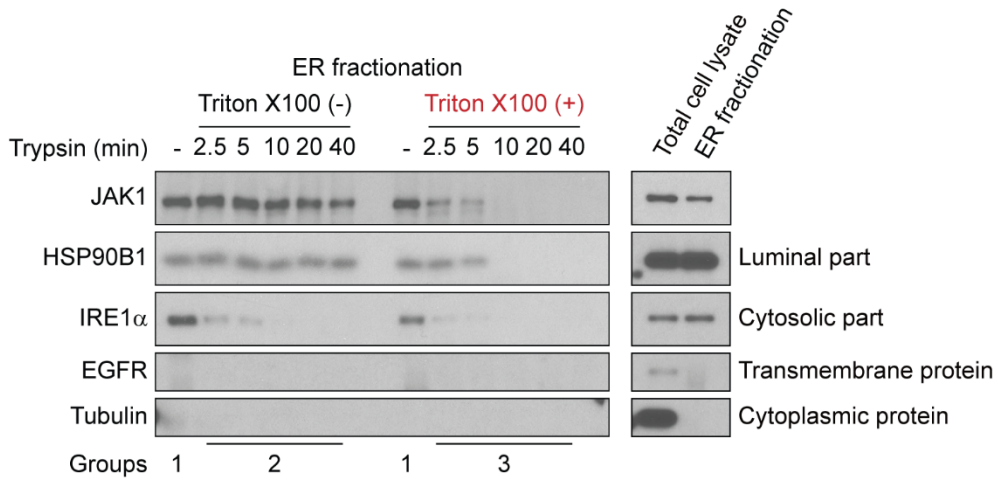

Figure 31. JAK1 is located in ER lumen in Hep 3B cells.

Trypsin digestion of ER fractions with (group 3) or without (group 2) permeabilization in Hep 3B cells.

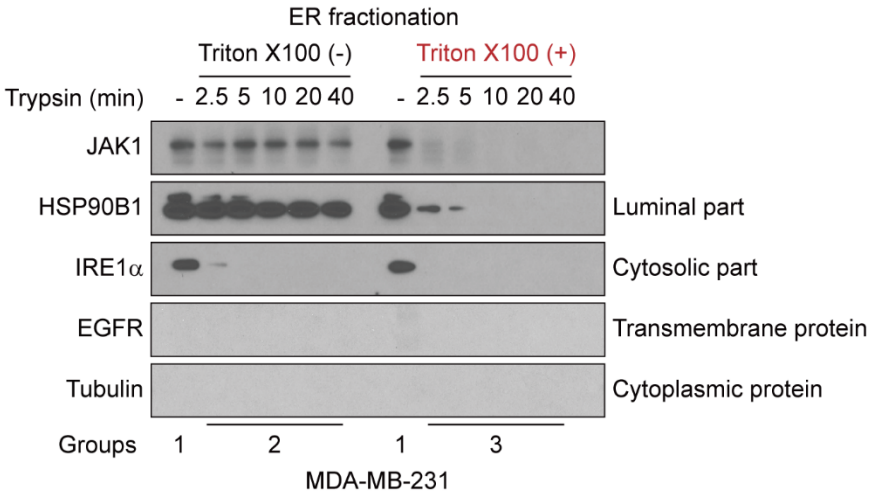

Figure 32. JAK1 is located in ER lumen in MDA-MB-231 cells.

Trypsin digestion of ER fractions without (group 2) or with permeabilization (group 3) in MB-231 cells.

3.5 JAK1 phosphorylates PD-L1 at Y112 to enhance STT3A association with PD-L1 and induces glycosylation of PD-L1 to maintain its protein stability

After validating that JAK1 interacts with ngPD-L1, we further tested our hypothesis that JAK1 directly phosphorylates ngPD-L1. We performed an *in vitro* kinase assay and detected Tyr-phosphorylation sites on immunoprecipitated exogenous PD-L1 from cells via mass spectrometric analysis. Result from *in vitro* kinase assay suggested that recombinant ngPD-L1 was strongly phosphorylated by JAK1 (Figure 33). Mass spectrometric analysis also identified only one Tyr-phosphorylation site (Y112) on PD-L1, which is a highly conserved residue across different species (Figure 34). Mutation of PD-L1 Y112 to phenylalanine (F) abrogated phosphorylation as shown by an *in vitro* kinase assay (Figure 35, lane 3 *vs*. 5). To recapitulate IL-6/JAK1-mediated phosphorylation of PD-L1 Y112 (pY112) *in vivo*, we generated two monoclonal antibodies against PD-L1 pY112, 10A5.2 and 6G3.1 (Figure 36). Higher levels of phosphorylated ngPD-L1 were pulled down from cells using both PD-L1 pY112 antibodies under IL-6 stimulation. In contrast, treatment with ruxolinitib or phosphorylated Y112 PD-L1 blocking peptide (hot peptide) abrogated the increase in IL-6–mediated phosphorylation of ngPD-L1 Y112 (Figure 37). These results indicated that IL-6–activated JAK1 phosphorylates ngPD-L1 at Y112.

To determine whether PD-L1 pY112 is required for IL-6/JAK1-induced PD-L1 stability through glycosylation, we generated Flag-PD-L1-Y112F-expressing HCC cells by the above-described dual expression method (Figure 2). Notably, exogenous PD-L1 protein expression was significantly reduced in the Y112F cells (Figure 38 and Figure 39). Moreover, the Y112F mutation did not affect the protein expression in ngPD-L1 (Figure 38). These results further supported that Y112 is required to maintain protein stability in glycosylation steps. Consistent with our results described above, PD-L1 mRNA level was not affected by the

Y112F mutation (Figure 40). As expected, IL-6 stimulation and/or treatment with ruxolinitib had no effect on the levels of total PD-L1 Y112F protein (Figure 39, lanes 7–10) or membrane-bound PD-L1 Y112F (Figure 41) compared with their effects on PD-L1 WT expression (Figure 39, lanes 1-6 and Figure 41). However, treatment with MG132 increased PD-L1 Y112F protein expression (Figure 41, lanes 12 *vs*. 7). Taken together, these results suggested that the IL-6/JAK1 pathway requires Y112 phosphorylation to maintain PD-L1 stability via glycosylation.

The results above indicated that STT3A enhances PD-L1 protein expression via the IL-6/JAK1 pathway and associates with phosphorylated ngPD-L1 (Figure 23 to 25). Compared with PD-L1 WT, binding of STT3A to the PD-L1 Y112F mutant was substantially reduced, supporting the notion that IL-6/JAK1-phosphorylated PD-L1 at Y112 recruits STT3A for glycosylation (Figure 42). Given that glycosylation is required to maintain PD-L1 stability by preventing its ubiquitination (52), we also examined the turnover rates of PD-L1 treated with or without ruxolinitib and PD-L1 Y112F mutant in both HA59T and Hep 3B HCC cells. The results indicated that Y112F mutation or ruxolinitib treatment induced faster turnover of PD-L1 compared with control (Figure 43 and Figure 44). Consistently, we detected more ubiquitination of PD-L1 Y112F than PD-L1 WT in the presence of MG132 (Figure 45). These results suggested that PD-L1 Y112 phosphorylation plays an important role for its interaction with STT3A, glycosylation initiation process, and subsequent protein stabilization.

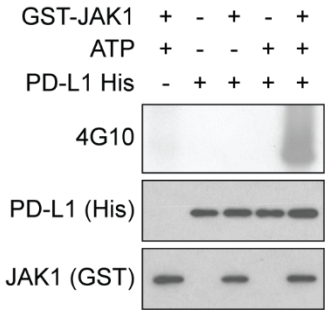

Figure 33. JAK1 directly phosphorylates ngPD-L1.

Recombinant ngPD-L1 protein from the pET 21a system was subjected to an *in vitro* kinase assay under the indicated conditions followed by Western blot analysis to detect Tyr phosphorylation using 4G10 antibody.

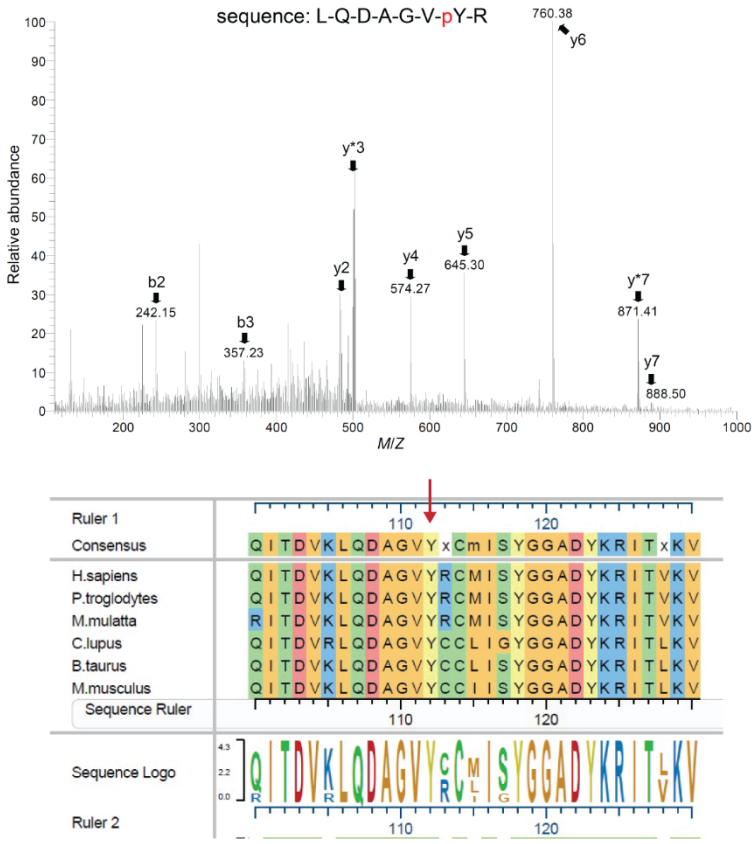

Figure 34. Tyrosine 112 of PD-L1 is phosphorylated.

Tyrosine 112 phosphorylation of PD-L1 was detected by liquid chromatography-tandem mass spectrometric analysis. Sequence alignment of Y112 PD-L1 across different species.

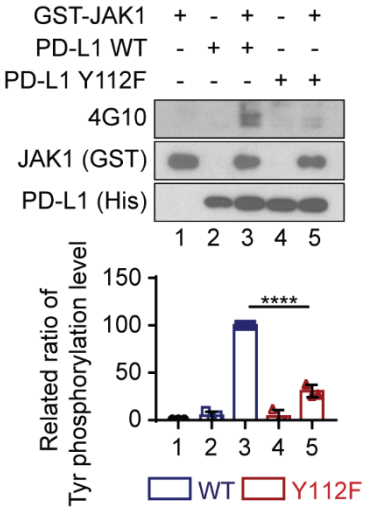

Figure 35. JAK1 directly phosphorylates PD-L1 at Y112 in *in vitro*.

In vitro kinase assay and WB analysis of tyrosine phosphorylation (4G10) of recombinant PD-L1 WT and PD-L1 Y112F protein.

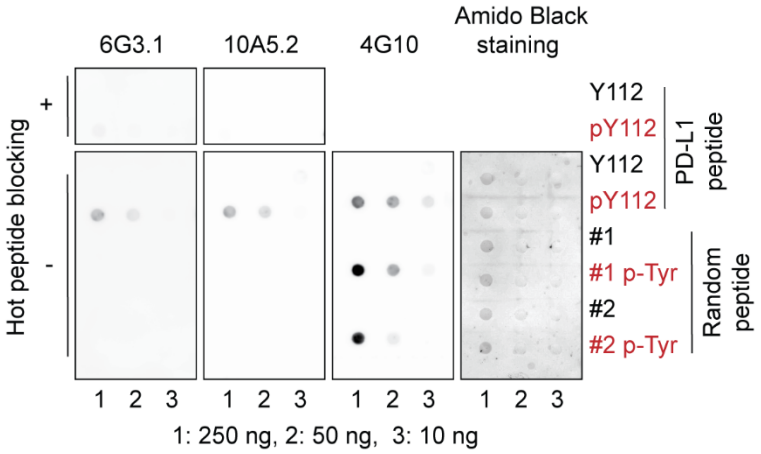

Figure 36. Antibody 10A5.2 and 6G3.1 detect PD-L1 Y112 phosphorylation in dot blots. Characterization of the PD-L1 pY112 antibodies generated by dot blotting. The antibody specifically recognizes the hot peptide (pY112) but not the cold peptide (Y112) or the other random peptides with Tyr phosphorylation (p-Tyr). This specific reaction of the PD-L1 pY112 antibody was completely neutralized by excessive amount of the PD-L1 pY112 hot peptide. 4G10 antibody was used to detect p-Tyr on pY112 PD-L1 peptide, random #1 and #2 peptide. Amido black staining was performed to show peptides on the nitrocellulose membrane.

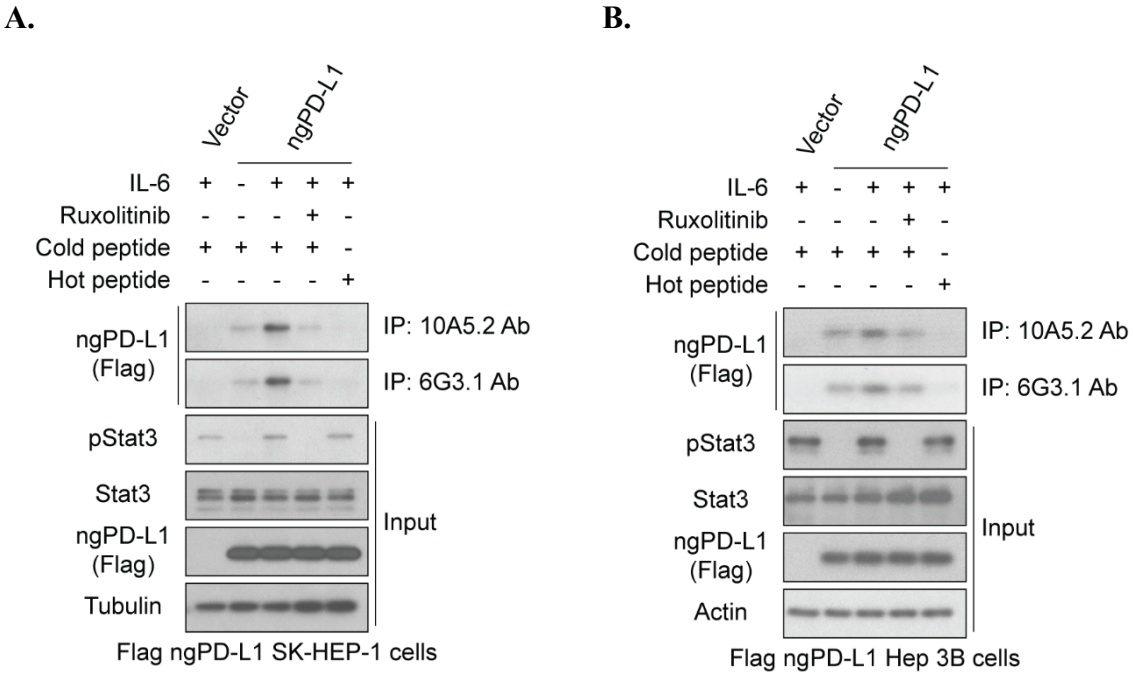

Figure 37. Antibody 10A5.2 and 6G3.1 detect PD-L1 Y112 phosphorylation in cells.

Cell lysates were subjected to immunoprecipitation (IP) followed by WB analysis to determine PD-L1 protein levels in SK-HEP-1 (A) or Hep3B (B) ngPD-L1 cells treated with or without IL-6 (20 ng/ml, 30 min) and ruxolitinib (10 μmol/L, 30 min) using the indicated antibodies, which were preincubated with cold or hot PD-L1 peptides (pY112).

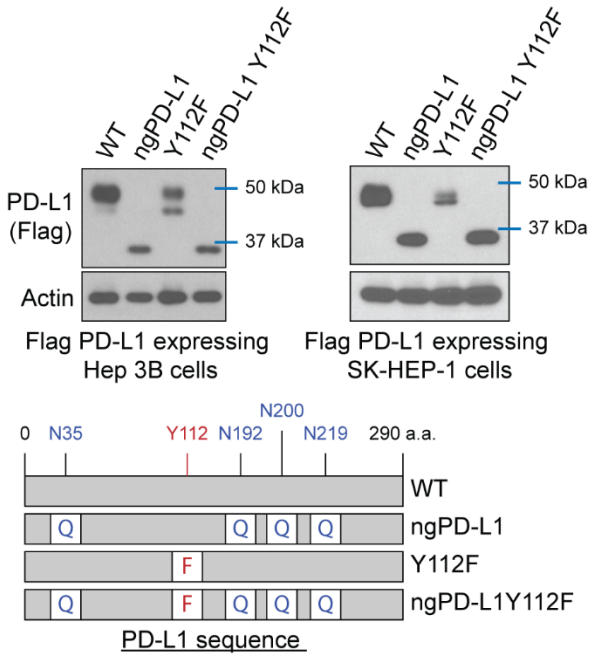

Figure 38. Y112F mutation only reduce PD-L1 protein stability but not ngPD-L1 in cells

WB analysis of lysates from each cells. Schematic diagram of various PD-L1 mutants used in this study. The numbers indicate amino acid positions on the PD-L1.

A.

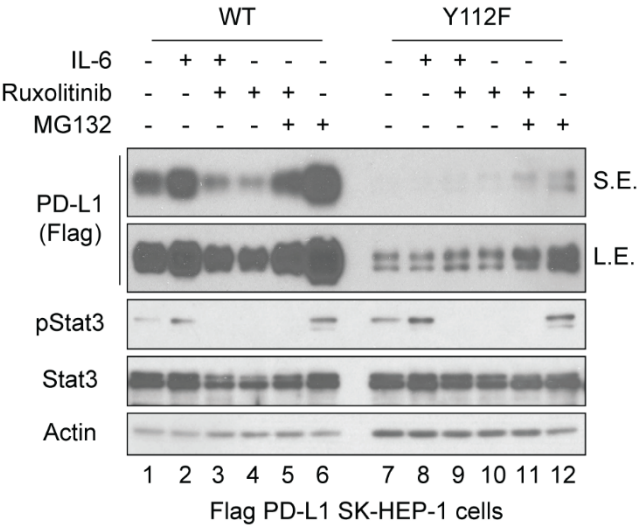

B.

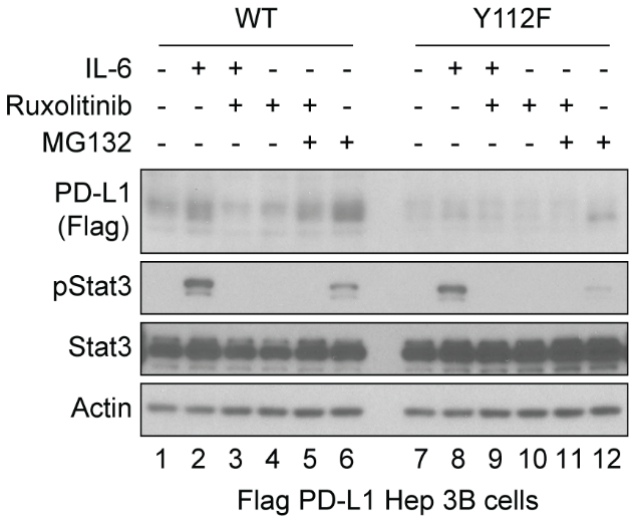

Figure 39. IL-6/JAK1 pathway upregulate PD-L1 WT protein expression but not Y112F mutation protein in HCC cancer cells.

WB analysis of exogenous PD-L1 expression in Flag-PD-L1 WT or Y112F in SK-HEP-1 (A) or Hep 3B (B) cells with or without exposure to IL-6 (20 ng/ml, 18 h), ruxolitinib (10 μmol/L, 18 h), and/or MG132 (10 μmol/L, 6 h). S.E., short exposure; L.E., long exposure**.**

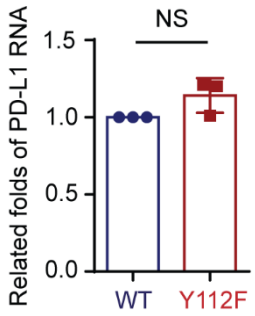

Figure 40. RNA expression level of PD-L1 WT or Y112F in Hep 3B cells.

Quantitative RT-PCR analysis of RNA from PD-L1 WT and PD-L1 Y112F Hep 3B cells. Three times independent experiments were performed. Error bars, mean ± S.D. NS, not significant, Mann-Whitney test.

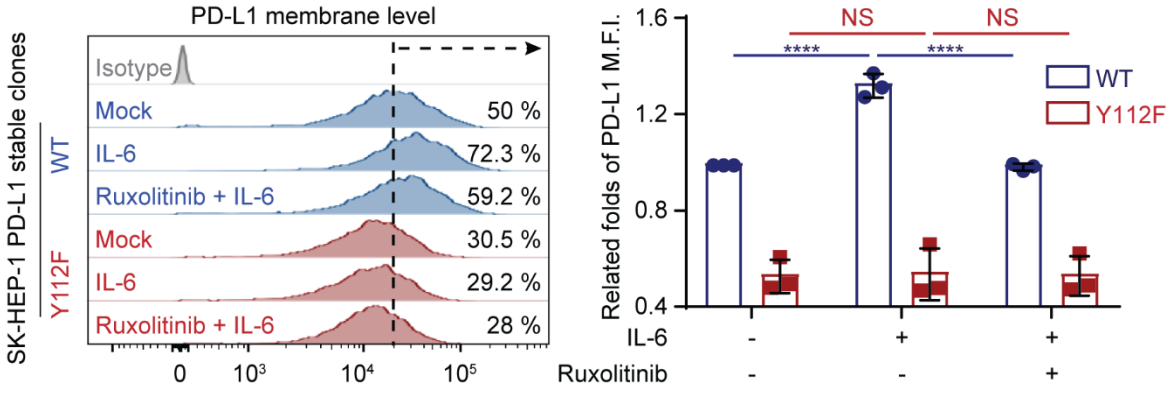

Figure 41. Surface level of PD-L1 WT or Y112F in SK-HEP-1 cells

Flow cytometric analysis of cell surface PD-L1 level in Flag PD-L1 WT- SK-HEP-1 or Y112F-SK-HEP-1 cells with or without exposure to IL-6 and/or ruxolitinib ($n = 3$). The relative fold-change in the mean fluorescence intensity (M.F.I.) of PD-L1 is shown. Error bars, mean ± S.D. ****$P < 0.0001$, NS, not significant, one-way ANOVA.

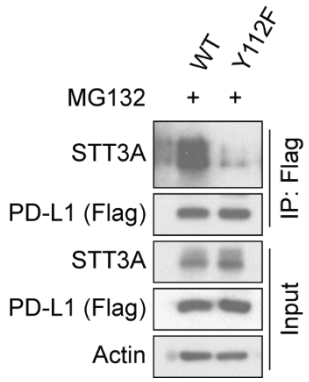

Figure 42. Losing PD-L1 Y112 phosphorylation reduces STT3A association.

Flag-PD-L1 WT or Y112F transfected 293T cells with exposure to MG132 (10 μmol/L, 6 h) were subjected to IP followed by WB analysis to determine the STT3A levels with the indicated antibodies.

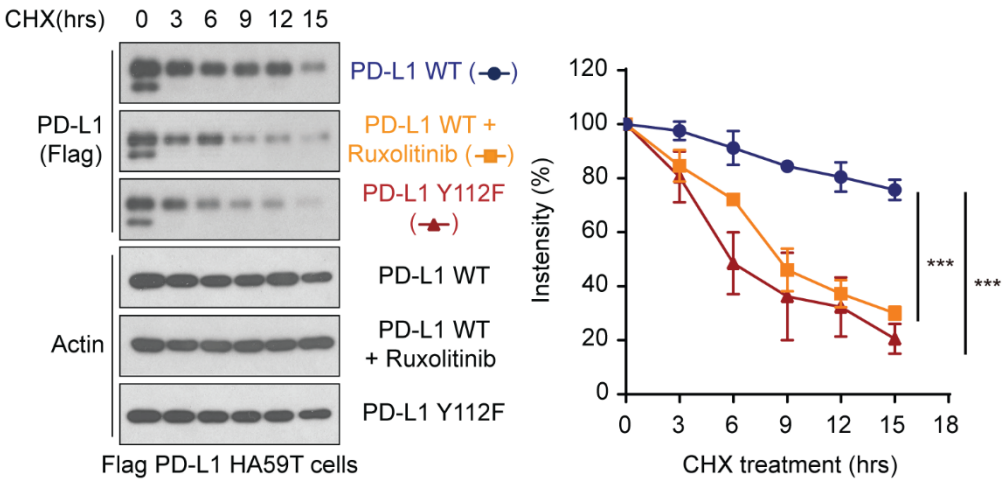

Figure 43. Y112F mutation or ruxolinitib treatment induced faster turnover of PD-L1 in HA-59T cells

Cycloheximide (CHX; 50 μmol/L) chase assays of PD-L1 protein turnover rates in Flag-PD-L1 WT-HA59T cells treated with or without ruxolitinib (10 μmol/L) and Flag PD-L1 Y112F-HA59T cells without ruxolitinib by WB analysis ($n = 3$). Error bars, mean ± S.D. ***$P < 0.001$, repeated-measures analysis of variance [ANOVA] with Tukey's post-hoc honest significant difference test.

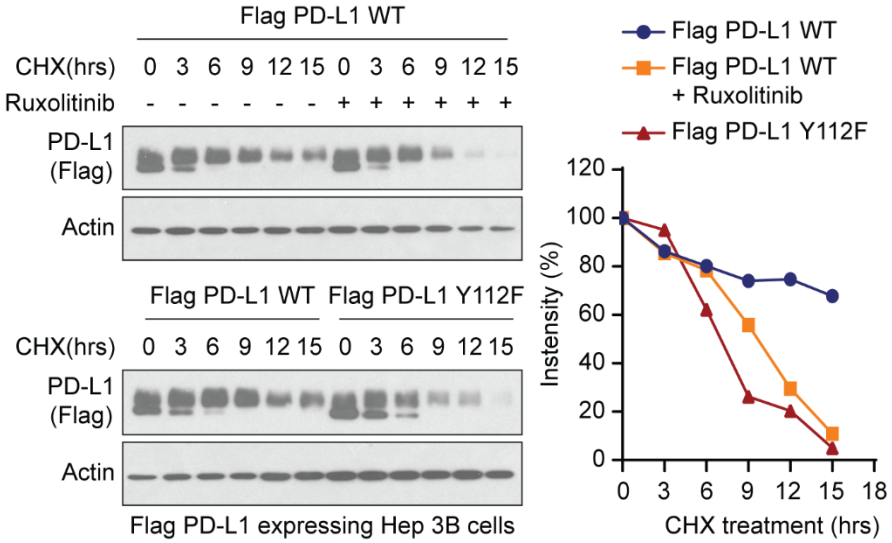

Figure 44. Y112F mutation or ruxolinitib treatment induced faster turnover of PD-L1 in Hep 3B cells.

WB analysis of Flag PD-L1 WT- or Y112F-Hep 3B cells treated with cycloheximide (CHX; 50 μM) or ruxolitinib (10 μM) for the indicated times.

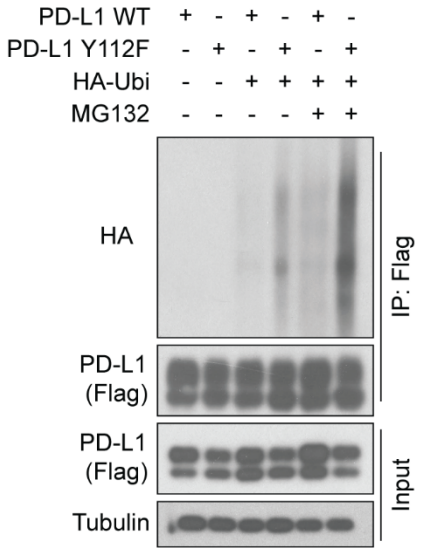

Figure 45. Increased ubiquitination in PD-L1 Y112F protein.

WB analysis of PD-L1 WT and Y112F protein ubiquitination level in 293T cells treated with or without MG132 (10 μmol/L, 6 h) with the indicated antibodies.

3.6 PD-L1 Y112 phosphorylation is required for liver cancer tumorigenesis in immunocompetent mice

Next, we asked whether PD-L1 Y112 phosphorylation governs PD-L1-driven cancer immune evasion *in vivo* and whether blocking the IL-6/JAK1/PD-L1 Y112 phosphorylation/STT3A signaling axis reduces PD-L1 expression level and enhances immune surveillance. To this end, we first generated Hepa 1-6 mouse hepatoma cells stably expressing PD-L1 WT or Y112F using the dual expression method. IL-6 stimulation and/or treatment with ruxolinitib had effect on the levels of total PD-L1 WT protein (Figure 46, lane 1-3) but not on Y112F mutation protein (Figure 46, lane 4-6). This result suggest Y112 phosphorylation is criticial for IL-6/JAK1-driven glycosylation and stabilization of PD-L1 in Hepa 1-6 cells.

To further validate the above phenomenon *in vivo*, we injected them into both immunodeficient (non-obese diabetic/severe combined immunodeficient, interleukin-2 receptor γ-chain (−/−) null [NSG] mice) and immunocompetent mice. The PD-L1 WT and Y112F Hepa 1-6 tumors from NSG mice exhibited similar growth and weight compared with WT tumors (Figure 47); however, the levels of PD-L1 expression were lower in the Y112F tumors than in WT tumors (Figure 48). In contrast, we observed striking tumor regression (Figure 49) and no relapsed tumors for over 11 months (Figure 50) in immunocompetent mice bearing PD-L1 Y112F compared with those with PD-L1 WT tumors. Moreover, more activated $CD8^+$ (granzyme B^+) T cells were present, and PD-L1 expression levels were much lower in Y112F tumors than that in WT tumors (Figure 51). Similar but less profound results were observed in mice bearing tumors derived from PD-L1 WT- or Y112F-expressing B16F10 melanoma cells (Figure 52). To further determine whether $CD8^+$ tumor-infiltrating lymphocytes (TILs)-driven killing effect is reduced by IL-6/JAK1/PD-L1 Y112 phosphorylation axis in cancer cells, we performed TILs co-culture assay using PD-L1 WT

and Y112F Hepa 1-6 cells (Figure 53). The PD-L1 WT Hepa 1-6 cells had increased survival rate under co-cultured with isolated and re-activated TILs in presence of IL-6 (Figure 53). This effect was abolished by the addition of PD-L1 neutralizing antibody. As expected, IL-6 stimulation had no effect on the survival of PD-L1 Y112F Hepa 1-6 cells co-cultured with TILs, supporting the critical role of the IL-6/JAK1/PD-L1 Y112 phosphorylation axis in cancer cell immune evasion from $CD8^+$ TILs. Together, these results indicated PD-L1 Y112 phosphorylation is crucial for maintaining PD-L1 stabilization and its immune checkpoint function. Therefore, blocking the IL-6/JAK1/PD-L1 Y112 phosphorylation signaling axis should reduce PD-L1 expression and enhance immune surveillance in the tumor microenvironment.

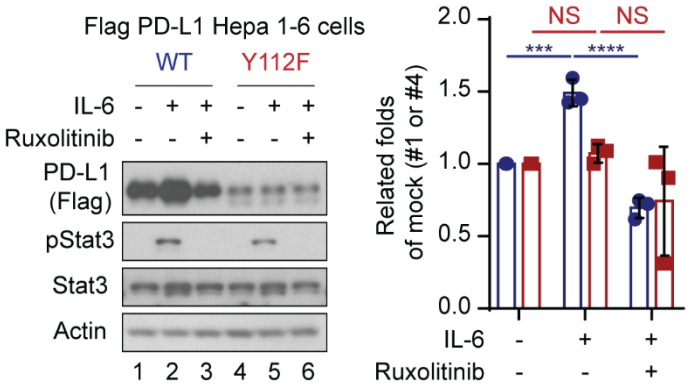

Figure 46. IL-6/JAK1 pathway upregulate PD-L1 WT protein expression but not Y112F mutation protein in Hepa 1-6 cells.

WB analysis of exogenous PD-L1 expression in Flag-PD-L1 WT or Y112F in Hepa 1-6 cells with or without exposure to IL-6 (20 ng/ml, 18 h) and ruxolitinib (10 μmol/L, 18 h). Error bars represent ± S.D. ***$P < 0.001$; ****$P < 0.0001$. one-way ANOVA.

A.

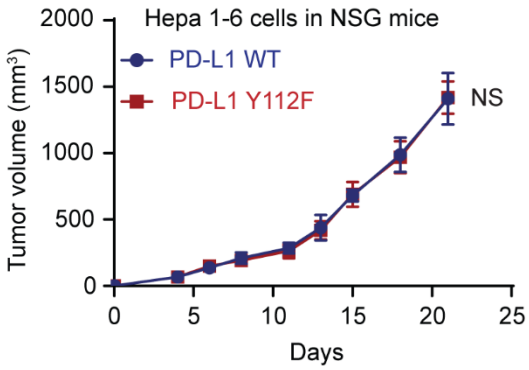

B.

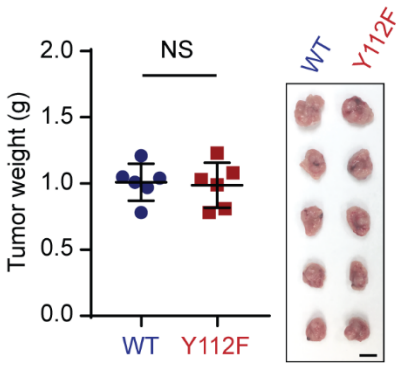

Figure 47. Tumorigenesis of PD-L1 WT and PD-L1 Y112F Hepa 1-6 cells in immunedeficient mice.

(A) Tumor growth of PD-L1 WT- Hepa 1-6 or Y112F-Hepa 1-6 cells in immunodeficient (NSG) mice ($n = 6$). (B) Tumor weight (left) and images of tumors (right) harvested from NSG mice inoculated with PD-L1 WT-Hepa 1-6 or Y112F- Hepa 1-6 cells. Scale bar, 1 cm. Error bars represent ± S.D. NS, not significant. Mann-Whitney test

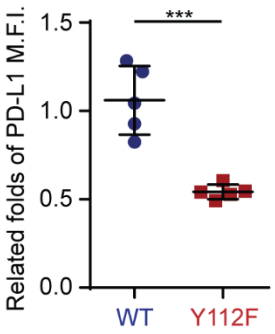

Figure 48. Surface level of PD-L1 WT and PD-L1 Y112F on Hepa 1-6 tumor.

Flow cytometric analysis of cell surface PD-L1 expression on PD-L1 WT- Hepa 1-6 or Y112F-Hepa 1-6 tumors (n = 5). The relative fold-change in the mean fluorescence intensity (M.F.I.) of PD-L1 is shown. Error bars represent ± S.D. ***P < 0.001, Mann-Whitney test.

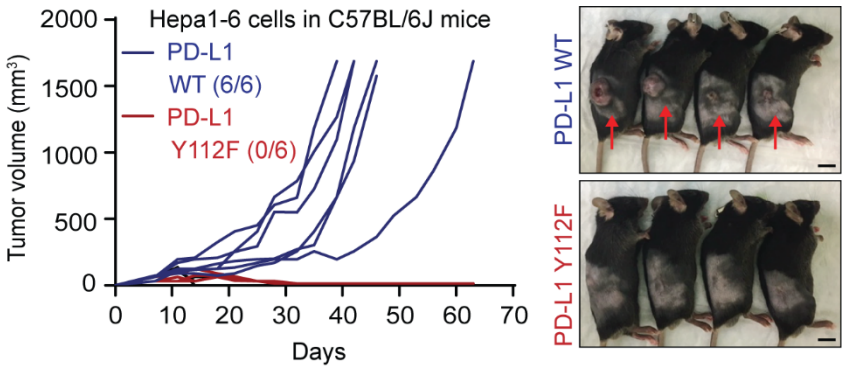

Figure 49. Tumorigenesis of PD-L1 WT and PD-L1 Y112F Hepa 1-6 cells in immunocompetent mice.

Individual tumor growth curves of PD-L1 WT- Hepa 1-6 or Y112F-Hepa 1-6 cells in immunocompetent (C57BL/6J) mice (n = 6).

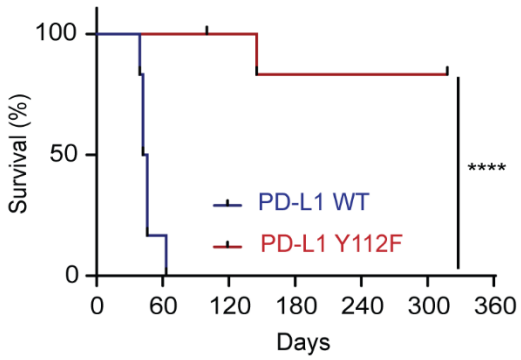

Figure 50. Survival curves of PD-L1 WT and PD-L1 Y112F Hepa 1-6 cells in immunocompetent mice.

Survival curves of PD-L1 WT- Hepa 1-6 or Y112F-Hepa 1-6 cells in immunocompetent (C57BL/6J) mice (n = 6). One mouse in the PD-L1 Y112F group died accidently at day 145. ****$P < 0.0001$, Log-rank Mantel-Cox test

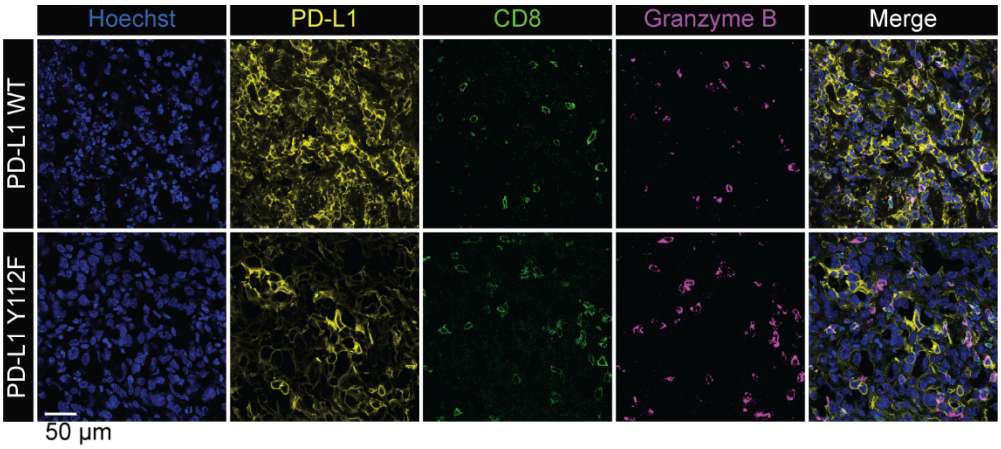

Figure 51. Population of activated CD8+ T cells in PD-L1 WT or Y112F Hepa 1-6 tumor microenvironment.

Representative immunofluorescence staining of PD-L1, CD8, and granzyme B expression in the indicated Hepa 1-6 stable cell-generated tumors.

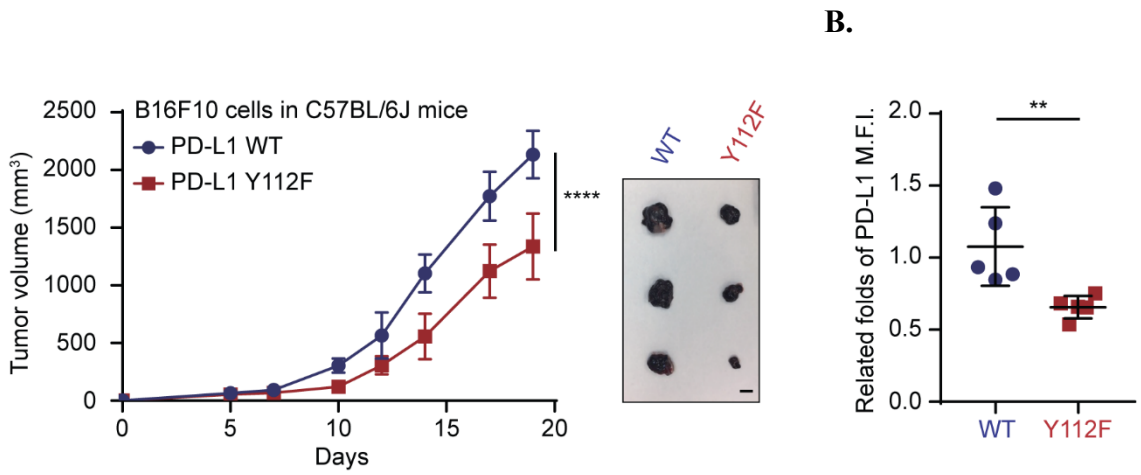

Figure 52. Tumor progression of PD-L1 WT and Y112F cells in B16F10 tumor bearing immunocompetent mice.

(A) Tumor growth and size of PD-L1 WT-B16F10 or Y112F-B16F10 tumors in immunecompetent mice ($n = 6$). (C) Flow cytometric analysis of cell surface PD-L1 from PD-L1 WT- B16F10 and Y112F- B16F10 tumors ($n = 5$). The relative fold change of the mean fluorescence intensity (M.F.I.) of PD-L1 is shown. Error bars, mean ± S.D. NS, not significant. $^{**}P < 0.01$; $^{****}P < 0.0001$, repeated-measures ANOVA in (A) and Mann-Whitney test in (B).

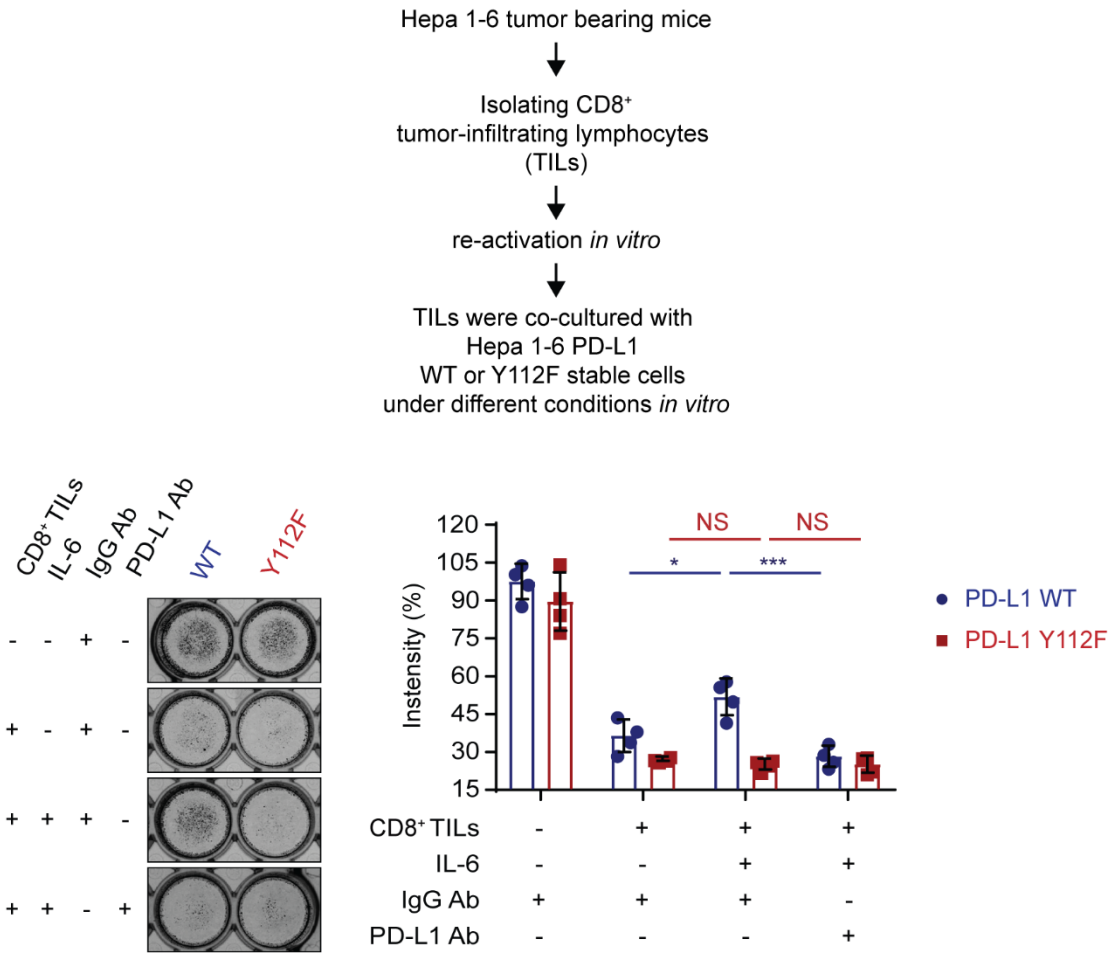

Figure 53. Growth ability of PD-L1 WT and Y112F Hepa-16 cells co-cultures with CD8$^+$ tumor-infiltrating lymphocytes (TILs).

TILs co-culture assay. Hepa 1-6 PD-L1 WT and Y112F cells were co-cultured with activated CD8$^+$ TILs from Hepa 1-6 tumor bearing mouse for 48 hr with or without IL-6 (20 ng/ml), PD-L1 antibody or IgG control antibody. Cells were subjected to crystal violet staining. (n = 4). Error bars represent ± S.D. *$P < 0.05$; ***$P < 0.001$. one-way ANOVA. NS, not significant.

3.7 Proposed working model how PD-L1 protein tyrosine phosphorylation, glycosylation initiation, and stability are regulated by the IL-6/JAK1 signaling pathway

Collectively, our results indicated that IL-6-activated JAK1 interacts with and phosphorylates non-glycosylated PD-L1 at Y112 residue in the ER where the Y112-phosphorylated PD-L1 increases its association with glycosyltransferase, STT3A, to initiate glycosylation. The glycosylated PD-L1 is stabilized and enhance the cancer immune escape from T cells in tumor microenvironment (Figure 54).

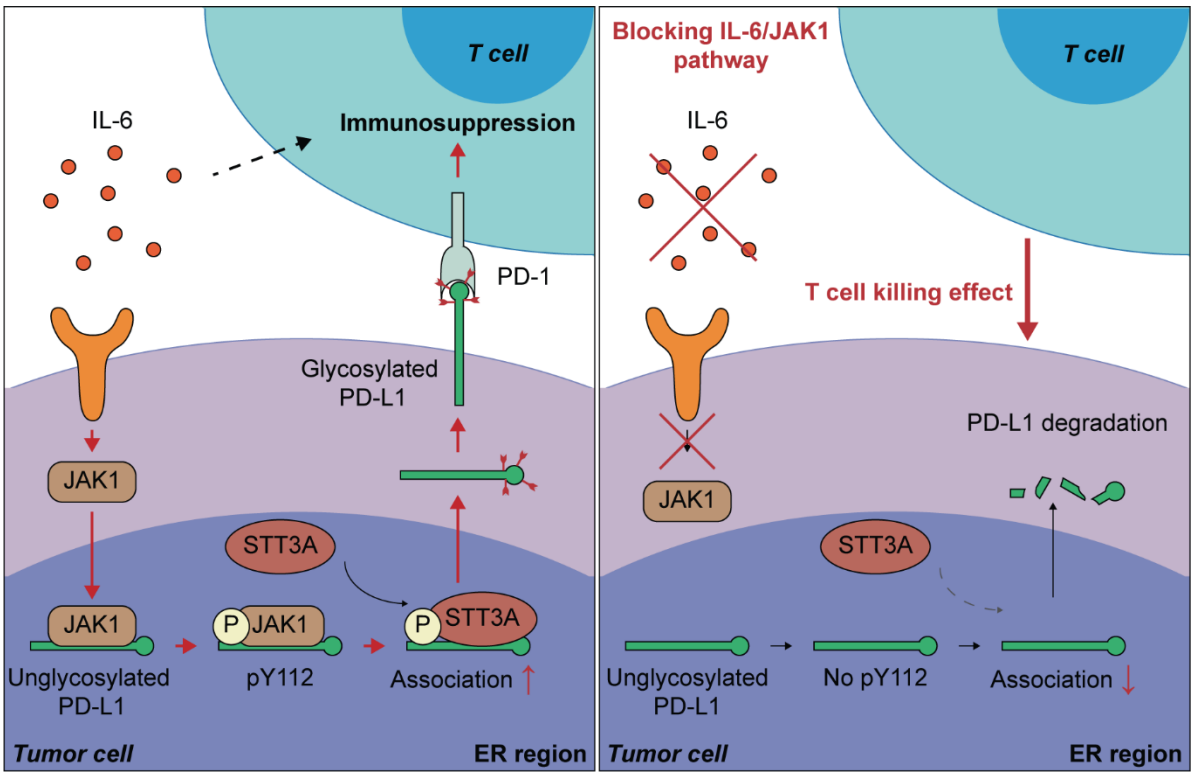

Figure 54. A proposed working model showing PD-L1 protein Y112 phosphorylation, glycosylation initiation, and stability regulated by the IL-6/JAK1 signaling pathway for cancer immune escape.

Under IL-6 stimulation, JAK1 interacts and phosphorylates non-glycosylated PD-L1 at Y112 in tumor cells, which enhances the association with STT3A for glycosylation initiation. Blocking the IL-6/JAK1 pathway leads to the loss of PD-L1 stability and sensitizes tumor cells to anti-Tim-3 immune checkpoint therapy.

CHAPTER 4. DISCUSSION

4.1 Significance and Conclusion

Due to there are limited treatment options for early or advantage stage of HCC patients, HCC is still the second most common cause of cancer death worldwide (63, 64). In patients with advanced HCC, the response rate to PD-1/PD-L1 blockade is approximately 20%. Thus, a deeper understanding of the biosynthesis of PD-L1 could result in the development of therapeutic strategies that may improve the efficacy of immunotherapy in this setting. . Previously, we reported that N-linked glycosylation of PD-L1 is required for maintaining PD-L1 stability and its interaction with PD-1 (52, 53, 56), and targeting PD-L1 with a glycosylation-specific antibody resulted in significant therapeutic benefit in a murine model of triple-negative breast cancer (51). However, the oncogenic signaling pathways initiating the glycosylation process of PD-L1 is not fully understood. Elucidating this mechanism may enhance the clinical effectiveness of current anti-PD-1/PD-L1 therapy through more specific patient selection or the development of novel, biomarker-driven combinatorial treatment approaches involving immunotherapeutic agents.

Here, we show that IL-6/JAK1 pathway-mediated tyrosine Y112 phosphorylation of PD-L1 is critical for the recruitment of N-glycosyltransferase, glycosylation initiation, protein stability, and subsequent cancer immune evasion. Blocking IL-6 downregulated PD-L1 expression and sensitized tumors to T cell killing. Thus, a deeper understanding of the mechanisms of glycosylation initiation of additional immune co-inhibitory molecules may lead to the development of more effective combinatorial treatment approaches to enhance the efficacy of immune checkpoint blockade.

In our study, we also showed that IL-6/JAK1/PD-L1 Y112 phosphorylation/STT3A signaling axis is required for liver tumorigenesis in immunocompetent mice (Figure 49 and 50). Importantly, increased expression of IL-6 is correlated with high PD-L1 expression in human HCC tumor tissue (Figure 11). Considering that the anti-PD-1 antibody, nivolumab, only achieves a response rate of 20% patients with advanced HCC, IL-6 could potentially serve as a biomarker predicting response to anti-PD-L1/PD-1 therapy in patients with HCC. Furthermore, previous studies have shown that IL-6 induces the expression of PD-1 in activated T cells, implying that reducing IL-6 expression in the tumor microenvironment may stimulate the anti-tumor immune response (7). Those studies and our current report together suggest that blocking the IL-6 pathway may abolish PD-L1/PD-1-driven cancer immune escape via different mechanisms in the tumor microenvironment (7, 65, 66) (model shown in Figure 53). This prompted us to further investigate a novel combinatorial treatment approach involving anti-IL-6 and -Tim-3 in murine models of liver cancer. Specifically, up to 80% of liver cancer-bearing mice responded to this combination without significant adverse effects (Figure 12 and 14). Because suppression of tumor growth and elevation of CTLs in the tumor region were also observed in aggressive B16F10 melanoma-bearing mice, the same therapeutic strategy may be generalized to other cancer types.

4.2 Oncogenic pathways for protein glycosylation in cancer

Glycosylation of proteins is a key regulatory step for governing several pathophysiological processes in cells. Despite recent progress providing more insight into the role of genomic alterations in tumorigenesis, there is still a limited understanding of the functional significance of the glycome and glycoproteome in cancer (67). Notably, specific glycan signatures present on tumor cells can be exploited as a target for blocking tumorigenesis.

In addition, aberrant glycosylation structures of oncoproteins can serve as neo-antigens for activating specific T cells (68). Indeed, the molecular pathways regulating protein glycosylation may contain novel therapeutic opportunities to enhance the efficacy of ICB for cancer patients.

Our study provides new insight into how oncogenic pathways directly orchestrate post-translational modification crosstalk to enhance glycoprotein generation, namely initiation of PD-L1 glycosylation by recruiting STT3A via JAK1-phosphorylated PD-L1. Employing this approach makes possible the identification of potential oncogenic pathways that amplify the ability of glycoproteins to enhance the malignant phenotypes of tumors. Although our study suggests that IL-6/JAK1 pathway-mediates tyrosine Y112 phosphorylation of PD-L1 and enhances the interaction of PD-L1 and STT3A, we cannot exclude the possibility that IL-6/JAK1/STAT pathway also upregulates the expression of other N-glycosyltransferases, which may accelerate the glycosylation process in tumor cells. To validate whether other members of the STAT family are also involved in PD-L1 post-translational modification or glycosylation and increase PD-L1 protein levels, we treated PD-L1-overexpressing cells with IL-6 and examined the expression levels of PD-L1 and the phosphorylation status of STAT1, STAT3, and STAT5. In our study, we only observed increased phosphorylation of STAT3 (Fig 55, Lane 1 and 2) but not STAT1 or STAT5. To further test whether activated STAT3 is involved in PD-L1 post-translational modification and enhances PD-L1 protein expression, we blocked the IL-6/JAK1/STAT3 pathway with ruxolinitib (JAK1 inhibitor) and HO-3867 (STAT3 inhibitor). Interestingly, enhanced levels of exogenous PD-L1 was abrogated only by ruxolinitib (Lane 2 vs. 3) but not HO-3867 (Lane 2 vs. 4), suggesting that the IL-6/JAK1

signaling axis we proposed in this study is the dominant mechanism responsible for the enhanced PD-L1 protein expression in tumor cells.

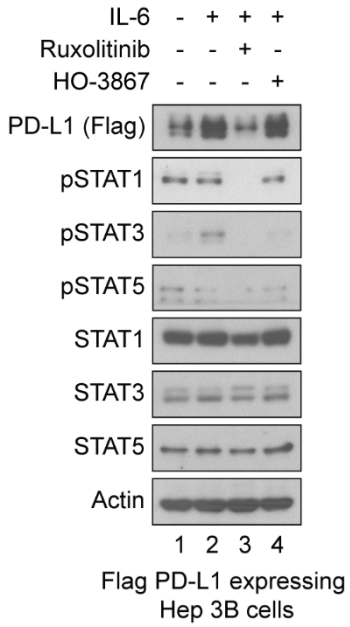

Figure 55. STAT family is not involved in IL-6/JAK1-driven PD-L1 upregulation.

WB analysis of cell lysates from Flag-ngPD-L1-Hep 3B cells with/without IL-6 stimulation exposure to IL-6 (20 ng/ml, 18 h), ruxolitinib (10 μmol/L, 18 h), and/or HO-3867 (10 μmol/L, 18 h).

4.3 PD-L1 biosynthesis in endoplasmic reticulum (ER)

Mechanisms of PD-L1 biosynthesis are tightly controlled by post-translational modifications, including phosphorylation, glycosylation, and ubiquitination, all of which are critical for stabilization of PD-L1 and immune escape (51, 52, 54, 55, 69, 70). However, the cellular location of PD-L1 phosphorylation and glycosylation in tumor cells remains unknown. In this study, we showed that JAK1 is a PD-L1 binding partner in the ER and Tyr phosphorylation on PD-L1 by the IL-6/JAK1 pathway is essential for PD-L1's association with N-glycosyltransferase, STT3A, which prevents ubiquitination and degradation of PD-L1. Although JAK1 has been shown to localize to the cytoplasmic membrane for JAK/STAT signaling pathway transduction and to the nucleus in epigenetic gene regulation by phosphorylating histone 3 Y41 as an oncoprotein (71-73), the current study further reveals its localization in the ER lumen to facilitate its interaction with PD-L1. Interestingly, we analyzed the JAK1 sequence using the software SignalP 4.1 (http://www.cbs.dtu.dk/services/SignalP/), and did not find an ER leader sequence on JAK1. However, when cells were stimulated by IL-6, we observed increased JAK1 proteins in the ER fraction and higher levels of phosphorylated ngPD-L1 was pulled down by the 6G3.1 antibody from the ER fraction (Figure 55). These results indicate that IL-6 may cause JAK1 to translocate to the ER, resulting in phosphorylation of ngPD-L1 Y112. In addition, the JAK family has been shown to be transported into the nucleus by a membrane receptor (71). Previous studies also demonstrate that membrane receptors can translocate into different cell organelles via retrograde trafficking pathways, i.e., from membrane to ER to nucleus (74, 75). These findings suggest a potential mechanism for the translocation of activated JAK1 to the other cellular compartments that would be worthwhile to explore in the future. In addition, we recently reported that metformin-activated

AMPK directly binds to and phosphorylates PD-L1 at Ser 195 in the ER. This event results in abnormal glycosylation of PD-L1 and leads to PD-L1 degradation via ER-associated protein degradation (ERAD) (56). A supply of ATP is required for kinase activation, but the catalysis of ATP uptake into the ER is still not fully understood. A recent study by Klein et al. reported that SLC35B1, also known as AXER (ATP/ADP exchanger in the ER membrane), maintains the ATP supply for protein biosynthesis in the ER (76), providing an explanation of how Tyr/Ser/Thr kinase gains ATP for their kinase activities in ER lumen. Together with our current findings, Tyr/Ser/Thr kinases can associate with PD-L1 in the ER and regulate PD-L1 glycosylation.

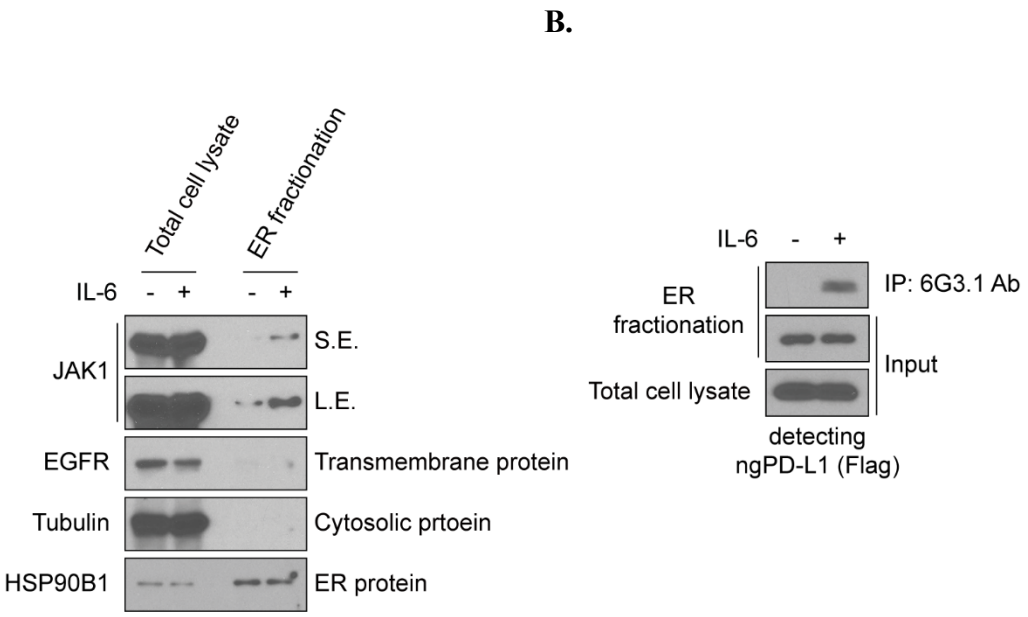

Figure 56. IL-6 causes JAK1 to translocate to the ER region and subsequent phosphorylation ngPD-L1 Y112

(A) WB analysis of total cell lysates or ER fractions from Flag-ngPD-L1-Hep 3B cells with/without IL-6 stimulation (20 ng/ml, 30 min). (B) Results of IP followed by WB analysis to determine ngPD-L1 pulled down levels in ER fractions from Flag-ngPD-L1-Hep 3B cells treated with or without IL-6 (20 ng/ml, 30 min) using the 6G3.1 antibodies.

4.4 Targeting IL-6/JAK1 for cancer immunotherapy

The IL-6/JAK/STAT3 pathway is aberrantly hyperactivated in multiple types of cancer and hyperactivation of this pathway is associated with a malignant phenotype and poor prognosis patients with cancer. Inhibitors of the IL□6/JAK/STAT3 pathway have demonstrated profound clinical benefit in patients with cancer by reducing tumor cell growth and stimulating the anti-tumor immune response (5, 7, 77, 78). In preclinical tumor mice models, inhibition of IL-6 in the tumor microenvironment results in enhanced efficacy of anti-PD-L1 (66, 79). Moreover, activation of JAK1 and JAK2 has been shown to upregulate the expression of immune checkpoint molecules (80, 81). However, loss of function of JAK family members contributes to the resistance of cancer to anti-CTLA4 and anti-PD-1 therapy by reducing neoantigen presentation and IFNγ-induced cancer cell apoptosis in patients (35, 82-84). Thus, direct inhibition of JAK1 kinase activity may disrupt immune surveillance in the tumor microenvironment. However, inactivation of IL-6 by a neutralization antibody in a combination with Tim-3 antibody has resulted in significant therapeutic efficacy. Recently, Miao et al. showed that *PBRM1* deficiency in tumors upregulates the IL-6/JAK/STAT3 pathway and was associated with a clinical benefit in patients with clear cell renal cell carcinoma receiving anti-PD-1 therapy (85). This phenomenon may be due to the activation of the IL-6/JAK pathway which in turn increases PD-L1 expression in tumor cells. Thus, blocking the PD-L1/PD-1 pathway may boost CTL activity in *PBRM1*-deficient cancer patients and further increase response rates. Treatment with immune checkpoint inhibitors has been shown to stimulate the production of IL-6 in serum, which can result in psoriasiform dermatitis, arthritis, and Crohn's disease in patients with cancer. Therefore, blocking the IL-6 pathway may reduce the severity of these side effects and extend the duration of immunotherapy (7).

4.5 Future direction

Overall, the mechanism of IL-6/JAK1-driven phosphorylation and glycosylation of PD-L1 leading to enhanced immune evasion in HCC provides a potential therapeutic target for a novel combinatorial treatment approach with an accompanying biomarker which may improve outcomes in HCC through better patient selection and enhanced therapeutic efficacy. This study also opens an avenue toward the understanding of how oncogenic kinases initiate protein glycosylation and amplify the ability of glycoproteins to enhance the malignant phenotypes of tumors.

The localization and function of activated JAK family has not been well characterized. Although once thought that JAK family proteins reside only in the cytoplasm, recent studies suggest that JAK1 and JAK2 exist in the nucleus of tumor cells and enhance cell proliferation (71, 72). Interestingly, our study found that JAK1 could also be isolated from the ER fraction and translocation of JAK1 into the ER could be stimulated by IL-6. ER–resident proteins contain a C-terminal KDEL-like motif for preventing secretion has been demonstrated. KDEL receptors localized in Golgi apparatus interact with protein with KDEL-like motif and triggers retrieval back to the ER via a coat protein I–dependent pathway (86). However, the amino acid sequence of JAK1 lacks an ER leader sequence or KDEL-like motif, implying that other mechanisms regulate the translocalization of JAK family under cytokine stimulation. Association with membrane receptors and translocation into different cell organelles via retrograde trafficking pathways is one potential mechanism. However, this current study only provides limited data in support of this hypothesis. Identifying the mechanism by which of member proteins and Ser/Thr/Tyr kinases translocate into the ER would open an avenue to

understand how kinases regulate the post-translational modification of oncoproteins in the ER by the signals from membrane receptor.

The tumor microenvironment is critical for promoting immune evasion and tumor recurrence. In our study, we utilized subcutaneous HCC and melanoma mouse models to assess the therapeutic efficacy of our proposed combinatorial treatment strategy. Since the subcutaneous HCC mouse model cannot completely mimic the liver tumor microenvironment, we should interpret with caution the therapeutic efficacy of the combination of anti-IL-6 and Tim-3 in our study. Since majority of liver cancers develop in the setting of chronic inflammatory conditions, like NASH or NAFLD, the design of suitable mouse models is fraught with multiple technical challenges (61). To test the efficacy of novel immunotherapeutic agents and their ability in preventing tumor recurrences, the spontaneous HCC mouse model with chemically-induced liver cirrhosis will be an important preclinical model for monitoring the response to therapy (87). This approach will also provide more detail of cancer immunogenomics and mechanism of immunotherapy resistance in future.

Bibliography

1. Marquardt JU, Andersen JB, and Thorgeirsson SS. Functional and genetic deconstruction of the cellular origin in liver cancer. *Nature reviews Cancer.* 2015;15(11):653-67.
2. Naugler WE, Sakurai T, Kim S, Maeda S, Kim K, Elsharkawy AM, and Karin M. Gender disparity in liver cancer due to sex differences in MyD88-dependent IL-6 production. *Science.* 2007;317(5834):121-4.
3. Park EJ, Lee JH, Yu GY, He G, Ali SR, Holzer RG, Osterreicher CH, Takahashi H, and Karin M. Dietary and genetic obesity promote liver inflammation and tumorigenesis by enhancing IL-6 and TNF expression. *Cell.* 2010;140(2):197-208.
4. He G, Dhar D, Nakagawa H, Font-Burgada J, Ogata H, Jiang Y, Shalapour S, Seki E, Yost SE, Jepsen K, Frazer KA, Harismendy O, Hatziapostolou M, Iliopoulos D, Suetsugu A, Hoffman RM, Tateishi R, Koike K, and Karin M. Identification of liver cancer progenitors whose malignant progression depends on autocrine IL-6 signaling. *Cell.* 2013;155(2):384-96.
5. Taniguchi K, and Karin M. IL-6 and related cytokines as the critical lynchpins between inflammation and cancer. *Semin Immunol.* 2014;26(1):54-74.
6. Hunter CA, and Jones SA. IL-6 as a keystone cytokine in health and disease. *Nature immunology.* 2015;16(5):448-57.
7. Johnson DE, O'Keefe RA, and Grandis JR. Targeting the IL-6/JAK/STAT3 signalling axis in cancer. *Nature reviews Clinical oncology.* 2018;15(4):234-48.
8. Michelotti GA, Machado MV, and Diehl AM. NAFLD, NASH and liver cancer. *Nature reviews Gastroenterology & hepatology.* 2013;10(11):656-65.

9. Llovet JM, Zucman-Rossi J, Pikarsky E, Sangro B, Schwartz M, Sherman M, and Gores G. Hepatocellular carcinoma. *Nature reviews Disease primers.* 2016;2(16018.

10. El-Serag HB. Hepatocellular carcinoma. *The New England journal of medicine.* 2011;365(12):1118-27.

11. Bruix J, Qin S, Merle P, Granito A, Huang YH, Bodoky G, Pracht M, Yokosuka O, Rosmorduc O, Breder V, Gerolami R, Masi G, Ross PJ, Song T, Bronowicki JP, Ollivier-Hourmand I, Kudo M, Cheng AL, Llovet JM, Finn RS, LeBerre MA, Baumhauer A, Meinhardt G, Han G, and Investigators R. Regorafenib for patients with hepatocellular carcinoma who progressed on sorafenib treatment (RESORCE): a randomised, double-blind, placebo-controlled, phase 3 trial. *Lancet.* 2017;389(10064):56-66.

12. Prieto J, Melero I, and Sangro B. Immunological landscape and immunotherapy of hepatocellular carcinoma. *Nature reviews Gastroenterology & hepatology.* 2015.

13. Pardoll DM. The blockade of immune checkpoints in cancer immunotherapy. *Nature reviews Cancer.* 2012;12(4):252-64.

14. Kalathil S, Lugade AA, Miller A, Iyer R, and Thanavala Y. Higher frequencies of GARP(+)CTLA-4(+)Foxp3(+) T regulatory cells and myeloid-derived suppressor cells in hepatocellular carcinoma patients are associated with impaired T-cell functionality. *Cancer research.* 2013;73(8):2435-44.

15. Li FJ, Zhang Y, Jin GX, Yao L, and Wu DQ. Expression of LAG-3 is coincident with the impaired effector function of HBV-specific CD8(+) T cell in HCC patients. *Immunology letters.* 2013;150(1-2):116-22.

16. Wang J, Sanmamed MF, Datar I, Su TT, Ji L, Sun J, Chen L, Chen Y, Zhu G, Yin W, Zheng L, Zhou T, Badri T, Yao S, Zhu S, Boto A, Sznol M, Melero I, Vignali DAA, Schalper K, and Chen L. Fibrinogen-like Protein 1 Is a Major Immune Inhibitory Ligand of LAG-3. *Cell.* 2019;176(1-2):334-47 e12.

17. Li H, Wu K, Tao K, Chen L, Zheng Q, Lu X, Liu J, Shi L, Liu C, Wang G, and Zou W. Tim-3/galectin-9 signaling pathway mediates T-cell dysfunction and predicts poor prognosis in patients with hepatitis B virus-associated hepatocellular carcinoma. *Hepatology.* 2012;56(4):1342-51.

18. Makarova-Rusher OV, Medina-Echeverz J, Duffy AG, and Greten TF. The yin and yang of evasion and immune activation in HCC. *Journal of hepatology.* 2015;62(6):1420-9.

19. Zou W, Wolchok JD, and Chen L. PD-L1 (B7-H1) and PD-1 pathway blockade for cancer therapy: Mechanisms, response biomarkers, and combinations. *Science translational medicine.* 2016;8(328):328rv4.

20. Sanmamed MF, and Chen L. A Paradigm Shift in Cancer Immunotherapy: From Enhancement to Normalization. *Cell.* 2018;175(2):313-26.

21. Shi F, Shi M, Zeng Z, Qi RZ, Liu ZW, Zhang JY, Yang YP, Tien P, and Wang FS. PD-1 and PD-L1 upregulation promotes CD8(+) T-cell apoptosis and postoperative recurrence in hepatocellular carcinoma patients. *International journal of cancer.* 2011;128(4):887-96.

22. Gao Q, Wang XY, Qiu SJ, Yamato I, Sho M, Nakajima Y, Zhou J, Li BZ, Shi YH, Xiao YS, Xu Y, and Fan J. Overexpression of PD-L1 significantly associates with tumor aggressiveness and postoperative recurrence in human hepatocellular carcinoma.

Clinical cancer research : an official journal of the American Association for Cancer Research. 2009;15(3):971-9.

23. El-Khoueiry AB, Sangro B, Yau T, Crocenzi TS, Kudo M, Hsu C, Kim TY, Choo SP, Trojan J, Welling THR, Meyer T, Kang YK, Yeo W, Chopra A, Anderson J, Dela Cruz C, Lang L, Neely J, Tang H, Dastani HB, and Melero I. Nivolumab in patients with advanced hepatocellular carcinoma (CheckMate 040): an open-label, non-comparative, phase 1/2 dose escalation and expansion trial. *Lancet.* 2017;389(10088):2492-502.

24. Wolchok JD, Chiarion-Sileni V, Gonzalez R, Rutkowski P, Grob JJ, Cowey CL, Lao CD, Wagstaff J, Schadendorf D, Ferrucci PF, Smylie M, Dummer R, Hill A, Hogg D, Haanen J, Carlino MS, Bechter O, Maio M, Marquez-Rodas I, Guidoboni M, McArthur G, Lebbe C, Ascierto PA, Long GV, Cebon J, Sosman J, Postow MA, Callahan MK, Walker D, Rollin L, Bhore R, Hodi FS, and Larkin J. Overall Survival with Combined Nivolumab and Ipilimumab in Advanced Melanoma. *The New England journal of medicine.* 2017;377(14):1345-56.

25. Postow MA, Chesney J, Pavlick AC, Robert C, Grossmann K, McDermott D, Linette GP, Meyer N, Giguere JK, Agarwala SS, Shaheen M, Ernstoff MS, Minor D, Salama AK, Taylor M, Ott PA, Rollin LM, Horak C, Gagnier P, Wolchok JD, and Hodi FS. Nivolumab and ipilimumab versus ipilimumab in untreated melanoma. *The New England journal of medicine.* 2015;372(21):2006-17.

26. Grivennikov SI, Greten FR, and Karin M. Immunity, inflammation, and cancer. *Cell.* 2010;140(6):883-99.

27. Toffanin S, Friedman SL, and Llovet JM. Obesity, inflammatory signaling, and hepatocellular carcinoma-an enlarging link. *Cancer cell.* 2010;17(2):115-7.

28. Crusz SM, and Balkwill FR. Inflammation and cancer: advances and new agents. *Nature reviews Clinical oncology.* 2015;12(10):584-96.

29. Elinav E, Nowarski R, Thaiss CA, Hu B, Jin C, and Flavell RA. Inflammation-induced cancer: crosstalk between tumours, immune cells and microorganisms. *Nature reviews Cancer.* 2013;13(11):759-71.

30. Taniguchi K, and Karin M. NF-kappaB, inflammation, immunity and cancer: coming of age. *Nature reviews Immunology.* 2018.

31. Yang X, Liang L, Zhang XF, Jia HL, Qin Y, Zhu XC, Gao XM, Qiao P, Zheng Y, Sheng YY, Wei JW, Zhou HJ, Ren N, Ye QH, Dong QZ, and Qin LX. MicroRNA-26a suppresses tumor growth and metastasis of human hepatocellular carcinoma by targeting interleukin-6-Stat3 pathway. *Hepatology.* 2013;58(1):158-70.

32. Shao YY, Lin H, Li YS, Lee YH, Chen HM, Cheng AL, and Hsu CH. High plasma interleukin-6 levels associated with poor prognosis of patients with advanced hepatocellular carcinoma. *Japanese journal of clinical oncology.* 2017;47(10):949-53.

33. Dhar D, Antonucci L, Nakagawa H, Kim JY, Glitzner E, Caruso S, Shalapour S, Yang L, Valasek MA, Lee S, Minnich K, Seki E, Tuckermann J, Sibilia M, Zucman-Rossi J, and Karin M. Liver Cancer Initiation Requires p53 Inhibition by CD44-Enhanced Growth Factor Signaling. *Cancer cell.* 2018;33(6):1061-77 e6.

34. Hanahan D, and Weinberg RA. Hallmarks of cancer: the next generation. *Cell.* 2011;144(5):646-74.

35. Sharma P, Hu-Lieskovan S, Wargo JA, and Ribas A. Primary, Adaptive, and Acquired Resistance to Cancer Immunotherapy. *Cell.* 2017;168(4):707-23.

36. Mahoney KM, Rennert PD, and Freeman GJ. Combination cancer immunotherapy and new immunomodulatory targets. *Nature reviews Drug discovery.* 2015;14(8):561-84.

37. Mellman I, Coukos G, and Dranoff G. Cancer immunotherapy comes of age. *Nature.* 2011;480(7378):480-9.

38. Li Y, Hermanson DL, Moriarity BS, and Kaufman DS. Human iPSC-Derived Natural Killer Cells Engineered with Chimeric Antigen Receptors Enhance Anti-tumor Activity. *Cell stem cell.* 2018;23(2):181-92 e5.

39. O'Donnell JS, Teng MWL, and Smyth MJ. Cancer immunoediting and resistance to T cell-based immunotherapy. *Nature reviews Clinical oncology.* 2018.

40. Melero I, Gaudernack G, Gerritsen W, Huber C, Parmiani G, Scholl S, Thatcher N, Wagstaff J, Zielinski C, Faulkner I, and Mellstedt H. Therapeutic vaccines for cancer: an overview of clinical trials. *Nature reviews Clinical oncology.* 2014;11(9):509-24.

41. Ribas A, Dummer R, Puzanov I, VanderWalde A, Andtbacka RHI, Michielin O, Olszanski AJ, Malvehy J, Cebon J, Fernandez E, Kirkwood JM, Gajewski TF, Chen L, Gorski KS, Anderson AA, Diede SJ, Lassman ME, Gansert J, Hodi FS, and Long GV. Oncolytic Virotherapy Promotes Intratumoral T Cell Infiltration and Improves Anti-PD-1 Immunotherapy. *Cell.* 2018;174(4):1031-2.

42. Chen L, and Han X. Anti-PD-1/PD-L1 therapy of human cancer: past, present, and future. *The Journal of clinical investigation.* 2015;125(9):3384-91.

43. Topalian SL, Taube JM, Anders RA, and Pardoll DM. Mechanism-driven biomarkers to guide immune checkpoint blockade in cancer therapy. *Nature reviews Cancer.* 2016;16(5):275-87.

44. Topalian SL, Drake CG, and Pardoll DM. Immune checkpoint blockade: a common denominator approach to cancer therapy. *Cancer cell.* 2015;27(4):450-61.

45. Coelho MA, de Carne Trecesson S, Rana S, Zecchin D, Moore C, Molina-Arcas M, East P, Spencer-Dene B, Nye E, Barnouin K, Snijders AP, Lai WS, Blackshear PJ, and Downward J. Oncogenic RAS Signaling Promotes Tumor Immunoresistance by Stabilizing PD-L1 mRNA. *Immunity.* 2017;47(6):1083-99 e6.

46. Casey SC, Tong L, Li Y, Do R, Walz S, Fitzgerald KN, Gouw AM, Baylot V, Gutgemann I, Eilers M, and Felsher DW. MYC regulates the antitumor immune response through CD47 and PD-L1. *Science.* 2016;352(6282):227-31.

47. Akbay EA, Koyama S, Carretero J, Altabef A, Tchaicha JH, Christensen CL, Mikse OR, Cherniack AD, Beauchamp EM, Pugh TJ, Wilkerson MD, Fecci PE, Butaney M, Reibel JB, Soucheray M, Cohoon TJ, Janne PA, Meyerson M, Hayes DN, Shapiro GI, Shimamura T, Sholl LM, Rodig SJ, Freeman GJ, Hammerman PS, Dranoff G, and Wong KK. Activation of the PD-1 pathway contributes to immune escape in EGFR-driven lung tumors. *Cancer discovery.* 2013;3(12):1355-63.

48. Parsa AT, Waldron JS, Panner A, Crane CA, Parney IF, Barry JJ, Cachola KE, Murray JC, Tihan T, Jensen MC, Mischel PS, Stokoe D, and Pieper RO. Loss of tumor suppressor PTEN function increases B7-H1 expression and immunoresistance in glioma. *Nature medicine.* 2007;13(1):84-8.

49. Cerezo M, Guemiri R, Druillennec S, Girault I, Malka-Mahieu H, Shen S, Allard D, Martineau S, Welsch C, Agoussi S, Estrada C, Adam J, Libenciuc C, Routier E, Roy S, Desaubry L, Eggermont AM, Sonenberg N, Scoazec JY, Eychene A, Vagner S, and

Robert C. Translational control of tumor immune escape via the eIF4F-STAT1-PD-L1 axis in melanoma. *Nature medicine.* 2018;24(12):1877-86.

50. RodrIguez E, Schetters STT, and van Kooyk Y. The tumour glyco-code as a novel immune checkpoint for immunotherapy. *Nature reviews Immunology.* 2018;18(3):204-11.

51. Li CW, Lim SO, Chung EM, Kim YS, Park AH, Yao J, Cha JH, Xia W, Chan LC, Kim T, Chang SS, Lee HH, Chou CK, Liu YL, Yeh HC, Perillo EP, Dunn AK, Kuo CW, Khoo KH, Hsu JL, Wu Y, Hsu JM, Yamaguchi H, Huang TH, Sahin AA, Hortobagyi GN, Yoo SS, and Hung MC. Eradication of Triple-Negative Breast Cancer Cells by Targeting Glycosylated PD-L1. *Cancer cell.* 2018;33(2):187-201 e10.

52. Li CW, Lim SO, Xia W, Lee HH, Chan LC, Kuo CW, Khoo KH, Chang SS, Cha JH, Kim T, Hsu JL, Wu Y, Hsu JM, Yamaguchi H, Ding Q, Wang Y, Yao J, Lee CC, Wu HJ, Sahin AA, Allison JP, Yu D, Hortobagyi GN, and Hung MC. Glycosylation and stabilization of programmed death ligand-1 suppresses T-cell activity. *Nature communications.* 2016;7(12632.

53. Hsu JM, Xia W, Hsu YH, Chan LC, Yu WH, Cha JH, Chen CT, Liao HW, Kuo CW, Khoo KH, Hsu JL, Li CW, Lim SO, Chang SS, Chen YC, Ren GX, and Hung MC. STT3-dependent PD-L1 accumulation on cancer stem cells promotes immune evasion. *Nature communications.* 2018;9(1):1908.

54. Zhang J, Bu X, Wang H, Zhu Y, Geng Y, Nihira NT, Tan Y, Ci Y, Wu F, Dai X, Guo J, Huang YH, Fan C, Ren S, Sun Y, Freeman GJ, Sicinski P, and Wei W. Cyclin D-CDK4 kinase destabilizes PD-L1 via cullin 3-SPOP to control cancer immune surveillance. *Nature.* 2018;553(7686):91-5.

55. Lim SO, Li CW, Xia W, Cha JH, Chan LC, Wu Y, Chang SS, Lin WC, Hsu JM, Hsu YH, Kim T, Chang WC, Hsu JL, Yamaguchi H, Ding Q, Wang Y, Yang Y, Chen CH, Sahin AA, Yu D, Hortobagyi GN, and Hung MC. Deubiquitination and Stabilization of PD-L1 by CSN5. *Cancer Cell.* 2016;30(6):925-39.

56. Cha JH, Yang WH, Xia W, Wei Y, Chan LC, Lim SO, Li CW, Kim T, Chang SS, Lee HH, Hsu JL, Wang HL, Kuo CW, Chang WC, Hadad S, Purdie CA, McCoy AM, Cai S, Tu Y, Litton JK, Mittendorf EA, Moulder SL, Symmans WF, Thompson AM, Piwnica-Worms H, Chen CH, Khoo KH, and Hung MC. Metformin Promotes Antitumor Immunity via Endoplasmic-Reticulum-Associated Degradation of PD-L1. *Molecular cell.* 2018;71(4):606-20 e7.

57. Wu TJ, Chang SS, Li CW, Hsu YH, Chen TC, Lee WC, Yeh CT, and Hung MC. Severe Hepatitis Promotes Hepatocellular Carcinoma Recurrence via NF-kappaB Pathway-Mediated Epithelial-Mesenchymal Transition after Resection. *Clinical cancer research : an official journal of the American Association for Cancer Research.* 2016;22(7):1800-12.

58. Kan Z, Zheng H, Liu X, Li S, Barber TD, Gong Z, Gao H, Hao K, Willard MD, Xu J, Hauptschein R, Rejto PA, Fernandez J, Wang G, Zhang Q, Wang B, Chen R, Wang J, Lee NP, Zhou W, Lin Z, Peng Z, Yi K, Chen S, Li L, Fan X, Yang J, Ye R, Ju J, Wang K, Estrella H, Deng S, Wei P, Qiu M, Wulur IH, Liu J, Ehsani ME, Zhang C, Loboda A, Sung WK, Aggarwal A, Poon RT, Fan ST, Wang J, Hardwick J, Reinhard C, Dai H, Li Y, Luk JM, and Mao M. Whole-genome sequencing identifies recurrent mutations in hepatocellular carcinoma. *Genome research.* 2013;23(9):1422-33.

59. Jang JW, Oh BS, Kwon JH, You CR, Chung KW, Kay CS, and Jung HS. Serum interleukin-6 and C-reactive protein as a prognostic indicator in hepatocellular carcinoma. *Cytokine.* 2012;60(3):686-93.

60. Flecken T, and Sarobe P. Tim-3 expression in tumour-associated macrophages: a new player in HCC progression. *Gut.* 2015;64(10):1502-3.

61. Brown ZJ, Heinrich B, and Greten TF. Mouse models of hepatocellular carcinoma: an overview and highlights for immunotherapy research. *Nature reviews Gastroenterology & hepatology.* 2018;15(9):536-54.

62. Breitling J, and Aebi M. N-linked protein glycosylation in the endoplasmic reticulum. *Cold Spring Harbor perspectives in biology.* 2013;5(8):a013359.

63. Luo X, and Feng GS. VEGFA genomic amplification tailors treatment of HCCs with sorafenib. *Cancer discovery.* 2014;4(6):640-1.

64. Zhu AX, Duda DG, Sahani DV, and Jain RK. HCC and angiogenesis: possible targets and future directions. *Nature reviews Clinical oncology.* 2011;8(5):292-301.

65. Wang LT, Chiou SS, Chai CY, Hsi E, Yokoyama KK, Wang SN, Huang SK, and Hsu SH. Intestine-Specific Homeobox Gene ISX Integrates IL6 Signaling, Tryptophan Catabolism, and Immune Suppression. *Cancer research.* 2017;77(15):4065-77.

66. Tsukamoto H, Fujieda K, Miyashita A, Fukushima S, Ikeda T, Kubo Y, Senju S, Ihn H, Nishimura Y, and Oshiumi H. Combined blockade of IL-6 and PD-1/PD-L1 signaling abrogates mutual regulation of their immunosuppressive effects in the tumor microenvironment. *Cancer research.* 2018.

67. Pinho SS, and Reis CA. Glycosylation in cancer: mechanisms and clinical implications. *Nature reviews Cancer.* 2015;15(9):540-55.

68. RodrIguez E, Schetters STT, and van Kooyk Y. The tumour glyco-code as a novel immune checkpoint for immunotherapy. *Nature reviews Immunology.* 2018.

69. Burr ML, Sparbier CE, Chan YC, Williamson JC, Woods K, Beavis PA, Lam EYN, Henderson MA, Bell CC, Stolzenburg S, Gilan O, Bloor S, Noori T, Morgens DW, Bassik MC, Neeson PJ, Behren A, Darcy PK, Dawson SJ, Voskoboinik I, Trapani JA, Cebon J, Lehner PJ, and Dawson MA. CMTM6 maintains the expression of PD-L1 and regulates anti-tumour immunity. *Nature.* 2017;549(7670):101-5.

70. Mezzadra R, Sun C, Jae LT, Gomez-Eerland R, de Vries E, Wu W, Logtenberg MEW, Slagter M, Rozeman EA, Hofland I, Broeks A, Horlings HM, Wessels LFA, Blank CU, Xiao Y, Heck AJR, Borst J, Brummelkamp TR, and Schumacher TNM. Identification of CMTM6 and CMTM4 as PD-L1 protein regulators. *Nature.* 2017;549(7670):106-10.

71. Zouein FA, Duhe RJ, and Booz GW. JAKs go nuclear: emerging role of nuclear JAK1 and JAK2 in gene expression and cell growth. *Growth factors.* 2011;29(6):245-52.

72. Rui L, Drennan AC, Ceribelli M, Zhu F, Wright GW, Huang DW, Xiao W, Li Y, Grindle KM, Lu L, Hodson DJ, Shaffer AL, Zhao H, Xu W, Yang Y, and Staudt LM. Epigenetic gene regulation by Janus kinase 1 in diffuse large B-cell lymphoma. *Proceedings of the National Academy of Sciences of the United States of America.* 2016;113(46):E7260-E7.

73. Buchert M, Burns CJ, and Ernst M. Targeting JAK kinase in solid tumors: emerging opportunities and challenges. *Oncogene.* 2016;35(8):939-51.

74. Chen MK, and Hung MC. Proteolytic cleavage, trafficking, and functions of nuclear receptor tyrosine kinases. *FEBS J.* 2015;282(19):3693-721.

75. Wang YN, Yamaguchi H, Hsu JM, and Hung MC. Nuclear trafficking of the epidermal growth factor receptor family membrane proteins. *Oncogene.* 2010;29(28):3997-4006.

76. Klein MC, Zimmermann K, Schorr S, Landini M, Klemens PAW, Altensell J, Jung M, Krause E, Nguyen D, Helms V, Rettig J, Fecher-Trost C, Cavalie A, Hoth M, Bogeski I, Neuhaus HE, Zimmermann R, Lang S, and Haferkamp I. AXER is an ATP/ADP exchanger in the membrane of the endoplasmic reticulum. *Nature communications.* 2018;9(1):3489.

77. Jones SA, and Jenkins BJ. Recent insights into targeting the IL-6 cytokine family in inflammatory diseases and cancer. *Nature reviews Immunology.* 2018.

78. Mauer J, Denson JL, and Bruning JC. Versatile functions for IL-6 in metabolism and cancer. *Trends in immunology.* 2015;36(2):92-101.

79. Mace TA, Shakya R, Pitarresi JR, Swanson B, McQuinn CW, Loftus S, Nordquist E, Cruz-Monserrate Z, Yu L, Young G, Zhong X, Zimmers TA, Ostrowski MC, Ludwig T, Bloomston M, Bekaii-Saab T, and Lesinski GB. IL-6 and PD-L1 antibody blockade combination therapy reduces tumour progression in murine models of pancreatic cancer. *Gut.* 2016.

80. Benci JL, Xu B, Qiu Y, Wu TJ, Dada H, Twyman-Saint Victor C, Cucolo L, Lee DSM, Pauken KE, Huang AC, Gangadhar TC, Amaravadi RK, Schuchter LM, Feldman MD, Ishwaran H, Vonderheide RH, Maity A, Wherry EJ, and Minn AJ. Tumor Interferon Signaling Regulates a Multigenic Resistance Program to Immune Checkpoint Blockade. *Cell.* 2016;167(6):1540-54 e12.

81. Prestipino A, Emhardt AJ, Aumann K, O'Sullivan D, Gorantla SP, Duquesne S, Melchinger W, Braun L, Vuckovic S, Boerries M, Busch H, Halbach S, Pennisi S,

Poggio T, Apostolova P, Veratti P, Hettich M, Niedermann G, Bartholoma M, Shoumariyeh K, Jutzi JS, Wehrle J, Dierks C, Becker H, Schmitt-Graeff A, Follo M, Pfeifer D, Rohr J, Fuchs S, Ehl S, Hartl FA, Minguet S, Miething C, Heidel FH, Kroger N, Triviai I, Brummer T, Finke J, Illert AL, Ruggiero E, Bonini C, Duyster J, Pahl HL, Lane SW, Hill GR, Blazar BR, von Bubnoff N, Pearce EL, and Zeiser R. Oncogenic JAK2(V617F) causes PD-L1 expression, mediating immune escape in myeloproliferative neoplasms. *Science translational medicine.* 2018;10(429).

82. Gao J, Shi LZ, Zhao H, Chen J, Xiong L, He Q, Chen T, Roszik J, Bernatchez C, Woodman SE, Chen PL, Hwu P, Allison JP, Futreal A, Wargo JA, and Sharma P. Loss of IFN-gamma Pathway Genes in Tumor Cells as a Mechanism of Resistance to Anti-CTLA-4 Therapy. *Cell.* 2016;167(2):397-404 e9.

83. Zaretsky JM, Garcia-Diaz A, Shin DS, Escuin-Ordinas H, Hugo W, Hu-Lieskovan S, Torrejon DY, Abril-Rodriguez G, Sandoval S, Barthly L, Saco J, Homet Moreno B, Mezzadra R, Chmielowski B, Ruchalski K, Shintaku IP, Sanchez PJ, Puig-Saus C, Cherry G, Seja E, Kong X, Pang J, Berent-Maoz B, Comin-Anduix B, Graeber TG, Tumeh PC, Schumacher TN, Lo RS, and Ribas A. Mutations Associated with Acquired Resistance to PD-1 Blockade in Melanoma. *The New England journal of medicine.* 2016;375(9):819-29.

84. Pan D, Kobayashi A, Jiang P, Ferrari de Andrade L, Tay RE, Luoma AM, Tsoucas D, Qiu X, Lim K, Rao P, Long HW, Yuan GC, Doench J, Brown M, Liu XS, and Wucherpfennig KW. A major chromatin regulator determines resistance of tumor cells to T cell-mediated killing. *Science.* 2018;359(6377):770-5.

85. Miao D, Margolis CA, Gao W, Voss MH, Li W, Martini DJ, Norton C, Bosse D, Wankowicz SM, Cullen D, Horak C, Wind-Rotolo M, Tracy A, Giannakis M, Hodi FS, Drake CG, Ball MW, Allaf ME, Snyder A, Hellmann MD, Ho T, Motzer RJ, Signoretti S, Kaelin WG, Jr., Choueiri TK, and Van Allen EM. Genomic correlates of response to immune checkpoint therapies in clear cell renal cell carcinoma. *Science.* 2018;359(6377):801-6.

86. Raykhel I, Alanen H, Salo K, Jurvansuu J, Nguyen VD, Latva-Ranta M, and Ruddock L. A molecular specificity code for the three mammalian KDEL receptors. *The Journal of cell biology.* 2007;179(6):1193-204.

87. Reiberger T, Chen Y, Ramjiawan RR, Hato T, Fan C, Samuel R, Roberge S, Huang P, Lauwers GY, Zhu AX, Bardeesy N, Jain RK, and Duda DG. An orthotopic mouse model of hepatocellular carcinoma with underlying liver cirrhosis. *Nature protocols.* 2015;10(8):1264-74.

Vita

Li-Chuan Chan was born in Hsinchu city in Taiwan. He received his Bachelor degree in veterinary medicine (BVM) at National Chung Hsing University (NCHU), Taiwan, after he finished his veterinary internship training at animal technology institute, NCHU veterinary teaching hospital and NCHU Animal disease diagnosis center in 2007. Then, he got his veterinary medicine license in 2007 and received the degree of Master of biopharmaceutical sciences at National Yang Ming University (NYMU), Taiwan in 2009. Upon completing his master's degree, he works as a veterinarian in Taiwan Technical Mission in Republic of Nauru, a subdivision of Taiwan International Cooperation and Development Fund, which also cooperated with the World Health Organization, the Taiwan government and the Nauru government. After one-year oversea veterinarian service, he worked as a research assistant in NYMU. In August of 2012, he entered The University of Texas MD Anderson Cancer Center UTHealth Graduate School of Biomedical Sciences for pursuing his Doctor of philosophy degree in cancer biology in Dr. Mien-Chie Hung's lab.